INFORMATION TO USERS

This manuscript has been reproduced from the microfilm master. UMI films the text directly from the original or copy submitted. Thus, some thesis and dissertation copies are in typewriter face, while others may be from any type of computer printer.

The quality of this reproduction is dependent upon the quality of the copy submitted. Broken or indistinct print, colored or poor quality illustrations and photographs, print bleedthrough, substandard margins, and improper alignment can adversely affect reproduction.

In the unlikely event that the author did not send UMI a complete manuscript and there are missing pages, these will be noted. Also, if unauthorized copyright material had to be removed, a note will indicate the deletion.

Oversize materials (e.g., maps, drawings, charts) are reproduced by sectioning the original, beginning at the upper left-hand corner and continuing from left to right in equal sections with small overlaps.

Photographs included in the original manuscript have been reproduced xerographically in this copy. Higher quality 6" x 9" black and white photographic prints are available for any photographs or illustrations appearing in this copy for an additional charge. Contact UMI directly to order.

Bell & Howell Information and Learning
300 North Zeeb Road, Ann Arbor, MI 48106-1346 USA
800-521-0600

A

SIMS Studies of Interfacial Effects in Polystyrene Thin Films

by

Yuri STRZHEMECHNY

A dissertation submitted to the Graduate Faculty in Physics in partial fulfillment of the requirements for the degree of ***Doctor of Philosophy***, The City University of New York

2000

This manuscript has been read and accepted for the Graduate Faculty in Physics in satisfaction of the dissertation requirement for the degree of Doctor of Philosophy.

6/15/00

Date

Professor Steven A. Schwarz, Advisor

Chair of Examining Committee

6/27/00

Date

Professor Louis Celenza

Executive Officer

Professor Azriel Z. Genack

Professor Alexander Lisyansky

Professor Miriam H. Rafailovich

SUNY, Stony Brook

Professor Jonathan Sokolov

SUNY, Stony Brook

Supervisory Committee

The City University of New York

Acknowledgements

It is a great pleasure for me to express my gratitude to the people without whose influence and help this work would not have come to its fruition. First and foremost to my supervisor Prof. Steven Schwarz, who had the patience to guide me through all the efforts and challenges, remaining my good friend and a true mentor in life and science. I have special gratitude towards Prof. Miriam Rafailovich who constantly supplied me with fresh and fruitful ideas and advices. I thank wholeheartedly Prof. Jonathan Sokolov for a constant keen interest in my research and invaluable help in conquering the fundamentals of polymer physics. My first graduate adviser, Prof. Narciso Garcia will always stay in my heart for his precious support during the first stages of my Ph.D. studies. He was the one who introduced me to the group that later became the core of the NSF Center named after him.

I thank Dr. Vladimir Zaitsev for all the time we spent together in long intellectual discussions and during short 'socializing' breaks. It was a joy to work next to my peers and co-authors Kungang Zhou, Vladimir Shapovalov, and Noppavan Chanunpanich. Our thanks to Dr. Fred Stevie at Lucent Technologies and Dr. David Simons at NIST, for providing the calibrated implantation standards used in this study. Laboratory assistance from Jonathan Schachter and Rashmi Kumar should be also gratefully acknowledged.

I must mention the name of Don van Duyne from Livsey Ananlytical, Inc. for all the wisdom he shared with me about hi-tech machinery for surface science and car racing competitions. Also, for the hardware/software aid and for the assistance in preparing illustrations for this thesis I express my special thanks to

Kaoru Yoshida.

This work was supported in part by the National Science Foundation, grant MRSEC, DMR-9632525.

Preface

The studies described herein utilize surface sensitive techniques to examine physical and chemical phenomena occurring in polymer materials on a submicron scale.

The targeted topic is relatively fresh in view of both fundamental and applied aspects. Polymers are currently seizing a place of extraordinary importance in everyday life. Their many fascinating properties are being extensively explored and utilized, yet still many issues remain open.

We address such properties of polymers as diffusion and preferential segregation. Special attention is paid to the peculiar role of surface and interfacial behavior.

These studies were performed in collaboration with several research groups in the Garcia Center (NSF Materials Research Science and Engineering Center: "Polymers at Engineered Interfaces"). The Center uses a number of modern instruments and techniques located in the Surface Studies Lab at Queens College. The facility is equipped with such tools as quadrupole and Time-Of-Flight (TOF) Secondary Ion Mass Spectrometry (SIMS), Auger Electron Spectroscopy (AES), X-Ray Photoelectron Spectroscopy (XPS), ellipsometry, profilometry, and rheology equipment.

The measurements run on the quadrupole SIMS instrument and their analysis comprise a central part of this thesis. Fundamentals and applications of SIMS will be described in separate sections. The samples under investigation are, primarily, thin (tens to hundreds of nanometers) films of both common and

specially synthesized polymers. These films and the wafers they sit on are treated in various chemical and thermal environments, and their properties are being monitored as a function of treatment parameters.

While many of the effects observed within such an approach have a sound theoretical background and may be rendered a straightforward explanation, still there are issues that require thorough study and deeper insight.

In Chapter 1, we will outline the experimental procedures and instrumentation involved. A brief introduction of the SIMS fundamentals will be given along with the main features of SIMS depth profiling. Several other surface and thin film analysis methods will be discussed. Description of the sample preparation routines will be provided as well.

Interfacial behavior of polymer melts is the primary focus of this work, and the current status of this subject will be reviewed in Chapter 2. We will survey the most important theoretical and experimental results obtained in this area recently and discuss open questions and problems pending.

Original results obtained for the interfacial dynamics in polymer thin films will be presented in Chapter 3. The main conclusion claimed is the observation of a non-trivial simultaneous scaling in space and time of the diffusion coefficient in a polymer melt.

The condition of the substrate surface has a great effect on the polymer chain behavior in thin films. Processing of silicon wafers as substrates for our studies was a substantial part of this thesis work. We examine the effects of wet etching techniques for these surfaces in Chapter 4.

In the last chapter we summarize other related results obtained with the

direct participation of the author in collaboration with other participants of the Garcia Center.

Contents

List of figures

CHAPTER 1

Experimental procedures

1.1. SIMS technique

The idea of Secondary Ion Mass Spectrometry is to induce emission of charged species (atomic ions and ionized clusters) from the surface under study by bombarding it with a beam of primary ions. The ejected secondaries are then discriminated over a wide range of masses inside a mass analyzer. The analysis may be performed in either static (the surface properties remain almost unaltered after bombardment), or dynamic mode (the material of the sample is being continuously sputtered away, revealing with time new subsurface layers). Although there exists a variety of different schemes of producing primary ion flow, a lot of ways to excite secondary ions from the surface, as well as a number of basic designs for a mass filter, all of them are incorporated into a general term - SIMS. SIMS finds extensive use in many fields of materials science, with parts per billion sensitivity, high (< 100 Å) depth resolution, decent (< 1 μ) lateral resolution, the ability to detect almost all elements and to be operated in different regimes (mass spectrum, depth profile, surface mapping, etc.).

The most common types of mass analyzers employed in SIMS instruments are the magnetic sector, quadrupole, and TOF (Time-Of-Flight). In magnetic sector instruments, secondary ions enter a region with a magnetic field where their trajectories are split by the Lorentz force due to a difference in masses. The

quadrupole mass detector employs filtering of particles' distance flown due to a combination of AC and DC electric fields applied inside of a four-rod configuration. TOF technique separates simultaneously emitted secondaries by the time they spend between emission and detection. All ions are initially given approximately the same kinetic energy, allowing lighter species to be detected ahead of the heavier ones.

Each of the listed mass filters has advantages and limitations. For a magnetic sector type, one can get a very good mass resolution (up to ten thousand), high sensitivity and throughput. Yet the mass filter itself has to have substantial dimensions, leading to certain vacuum concerns and additional cost. Quadrupole mass analyzers can be made much smaller, faster and cheaper. Quadrupole instruments also produce much lower contamination from sputtering and allow for the variable sample orientation, but they have lower transmission, mass resolution (in the hundreds), and sensitivity. TOF instruments, while having superb mass resolution and ability of detecting very high masses, are generally considered to lack the speed and the throughput of the first two mass spectrometer types.

Currently, at Queens College there are two SIMS facilities being operated: TOF-SIMS "CAMECA" and quadrupole "ATOMIKA ADIDA 3000-30". For the SIMS studies described in this thesis, we employed the "ATOMIKA" instrument in most cases. It is equipped with an ion gun, where the flux of primary ions may be extracted from a plasma of either oxygen or argon gas. These ions can then be accelerated to energies in the range 1 through 15 keV, focused and rastered across the surface of the sample. The sample is positioned on a carousel inside a main chamber with ultra-high vacuum conditions ($< 10^{-8}$ torr). The secondary ionized

species ejected from the sample are drawn into the secondary optics, followed by a quadrupole mass filter. The position of the sample relative to the detector opening can be adjusted by means of variation of the incline angle of a sample holder. An option of applying a constant voltage bias to the carousel stage is also available. An additional advantage in the setup is the presence of an electron gun that provides surface charge neutralization for samples while bombarded with primary ions. It has been found (see, for example Ref. 1) that for most polymer species, a practical operation scheme is 2 keV 30°-off normal Ar^+ bombardment, which was primarily being employed throughout all the runs in this work.

Depth profiling is one of the operating modes of SIMS. The idea is to monitor the intensity of the secondary ions as a function of time. As the sputtering of the material proceeds (a beam of primary ions is rastered across a square area of about 1 mm^2) a crater is created (see Fig. 1.1). If, for some reason, a concentration of a certain element at the crater bottom is changing with depth it will show up as a distinct change of the yield with time. As a rule, depth scales with the time of sputtering. The dependence of the concentration vs. depth is the depth profile.

The observed charged secondaries can be atomic or molecular (cluster) ions, both positive and negative. The choice of the masses to detect is based on a number of factors, empirical as well as fundamental. An important property of SIMS is the ability to distinguish between different isotopes of the same element. In conjunction with this, we shall mention that for polymers, isotope tagging (the most popular tag - a substitution of hydrogen with deuterium) opens almost unlimited experimental opportunities.

The SIMS technique involves certain difficulties though. The probability

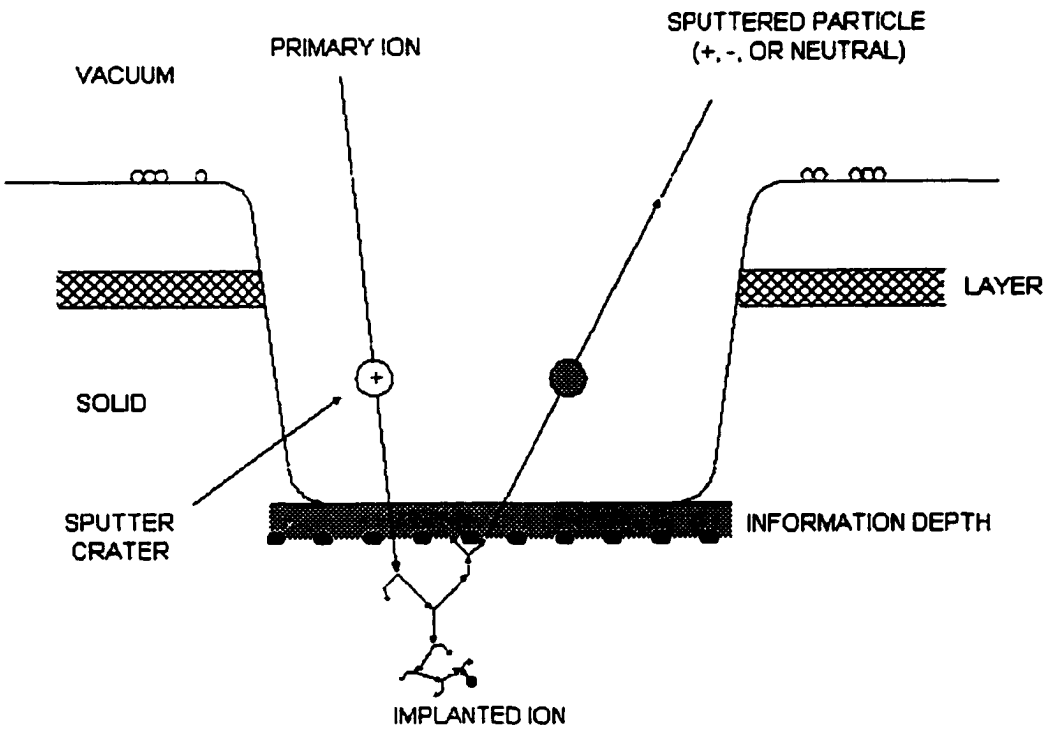

Figure 1.1 A schematic diagram of the SIMS in the depth profiling mode. The beam of primary ions results in secondary sputtered ionic species. Depth variation of the secondaries' concentration produces a change in their relative yield.

of ion formation is varying from element to element by orders of magnitude, thus making detection of some of them rather problematic. Also, there is an uncertainty in the species identification due to mass interference. For instance, ions of O_2 and S have the same mass 32 a.m.u., or CO and Si ions interfere at 28 a.m.u. Fortunately, there are ways to overcome these setbacks. TOF-SIMS detectors allow mass resolution well above the proton/neutron mass ratio, which effectively eliminates almost all the mass ambiguities. As far as the "ATOMIKA" instrument is concerned, it is equipped with an electron gun and a hemispherical energy analyzer. That provides an opportunity to run parallel energy detection of the secondary electrons. If the analyzer is tuned to the characteristic energies of the relevant Auger peaks (see the next section for details), another kind of depth profile (associated with the intensity of secondary electron flux) will be monitored. The two simultaneous runs - SIMS and Auger - complement each other. Another way of resolving mass detection ambiguities on the "ATOMIKA" is to apply a voltage bias to the stage. A change in the electric potential of the surface leads to a significant decrease in the escape probability for clusters, whereas for single atoms the ion yield is influenced only moderately.

At the crater edges, some signal uncertainty occurs due to a finite diameter of the ion beam. That may result in some unwanted background in the integrated yield. This problem of the edge effects is resolved by introducing electronic gating - the data is collected only in the central region of the crater.

When dielectric materials, polymers included, are treated on SIMS, they may gradually accumulate uncompensated charge. Usually it brings about an instability in the signal of secondaries - gradual decline alongside sharp jumps. But

if an unfocused electron beam is directed into the vicinity of the crater, the surface may be effectively neutralized.

A separate and very relevant problem of depth resolution should be mentioned. The conventional definition of depth resolution of a sharp interface is the depth within which the signal changes between 16 and 84 % of its maximum value. The most important factors affecting the depth resolution in SIMS profiling mode are: a) the atomic mixing in collision cascades; b) surface roughening evolving during bombardment; c) transient effects such as preferential sputtering of certain species occurring due to differences in surface binding energies, sputter escape depths, and energy transfers within the cascade; d) chemical interfacial segregation; e) radiation-enhanced effects, that can be thermal, defect-mediated, and charge-induced; and f) the quality of the sample. Currently, the best results obtained for the SIMS depth resolution on polymer samples are within several nanometers. In our studies, this issue is crucial, and we will return to it later.

1.2. Other instrumental techniques

SIMS depth profiling, although a powerful experimental method, sometimes cannot provide all the information sought. But when complemented by other techniques, the experiment can yield robust and unambiguous results. Often we are using, along with profiling, several standard and effective procedures to produce a broader spectrum of results and to obtain a clearer picture of the systems investigated.

The SIMS instruments themselves can provide an extended range of features. When the mass filter operates in a mode that continuously varies the

secondaries' detected mass, a mass spectrum of the surface species is obtained. The mass spectrum analysis enables one to get a clearer understanding of the surface composition and eliminate possible mass interferences. The SIMS imaging regime can also be helpful and informative. For this case, as the primary beam rasters across the surface, a compositional 'portrait' of the sample (two- or three-dimensional) is created. SIMS imaging, for polymers in particular, is very useful for resolving morphology of the sample, detecting phase boundaries, studying lateral kinetics and anisotropy.

Another surface-sensitive technique employed in our research group is X-Ray Photoelectron Spectroscopy (XPS); the measurement of binding energies of electrons ejected from a surface by a monoenergetic beam of soft X-rays. XPS can be used to determine the concentration of different chemical elements in the sample. Differences in binding energies, resulting from differences in chemical potential and polarizability, can be used for identification of distinct chemical states. The analyzer scans for different energies of incoming electrons and detects the intensity of electron flux for a given energy. As a result, an XPS energy spectrum is produced, where the intensity is plotted vs. emission energy. The main advantages of XPS are its non-destructive nature, sufficiently high sensitivity, ability to detect practically all elements and their chemical states. Another advantage of XPS is the limited information depth due to relatively short (several nm) escape depths of the secondary electrons. Figure 1.2 illustrates schematically a photon-electron interaction accompanying the XPS emission of a 1s line.

Alongside that process, the so-called Auger emission can occur, when the vacancy created by the removed XPS electron is filled with a high-level electron

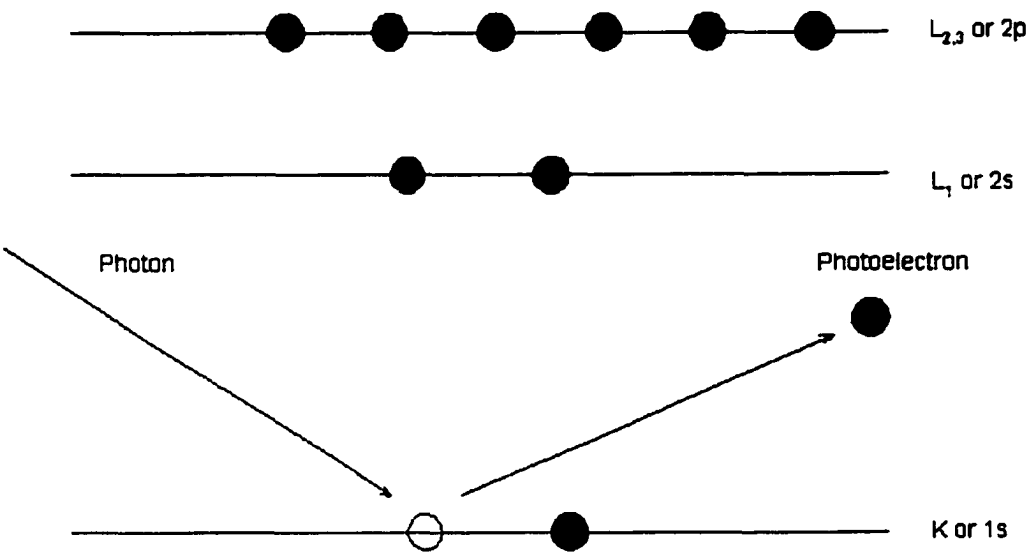

Figure 1.2 The process of the XPS photoelectron emission. A primary photon causes the ejection of the secondary electron.

relaxing with a simultaneous 'radiationless' ejection of another high-level electron. The diagram for this process is shown in Fig. 1.3. In principle, the Auger-effect can be generated by particles other than photons. Electron- and ion-induced Auger transitions can be detected within an appropriate setup.

The XPS instrument we have at our disposition is "KRATOS-ES300". It is equipped with an X-Ray gun running with Al and Mg target anodes, and a hemispherical analyzer for detecting electrons of various energies. The sampleholder is designed to have an adjustable angle for the electrons escaping from the surface into the detector.

For dielectric surfaces, polymers included, charging may produce certain accountable energy shifts, but does not pose as serious a problem as in SIMS.

As we mentioned before, the "ATOMIKA" instrument also has a hemispherical analyzer, capable of detecting electron- and ion-induced Auger-electrons. This feature becomes beneficial when the sample surface contains species with interfering masses.

For more fundamentals of XPS, Auger-electron spectroscopy, as well as SIMS, we refer the reader to [2].

When running a SIMS depth profile, the concentration of a given species is detected as a function of time. The sputtering rate may be known for a given surface, and one can rescale the time axis into depth. Nonetheless, very often this rescaling procedure introduces a substantial error, and more accurate methods are required.

One such routine utilizes ellipsometric measurements. The ellipsometer is an optical instrument measuring the changes in polarization of momochromatic

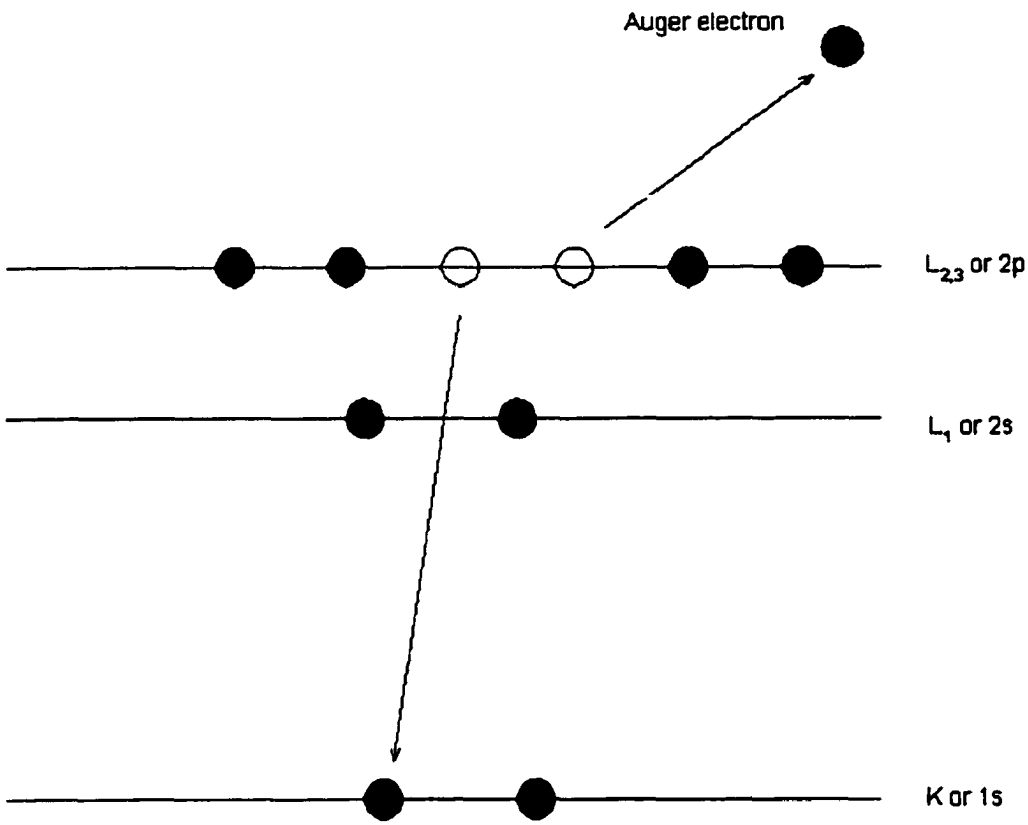

Figure 1.3 The Auger relaxation process resulting in the emission of a KLL electron and a final state with two vacancies.

polarized light reflected form a surface of interest. The comparison of the azimuth angles of polarization is performed for the incident and reflected beams. As a result, the information obtained allows a direct calculation of the real and imaginary part of the refractive index of the surface, and for the case of a reflective substrate covered with a transparent thin film, the thickness of the film. The advantageous characteristics of ellipsometry are its high (fraction of a nanometer) thickness resolution, capability of determining the index of refraction of an unknown substance, and the ability to yield results in various environments, open air included.

The thin polymer samples we investigate are usually transparent and permit rather straightforward and precise ellipsometric measurements. When a depth profile is generated, and a certain interface is reached (e.g. the boundary between the film and the solid substrate), subsequent ellipsometry data can be used for the direct rescaling of the number of SIMS raster cycles needed to reach the interface. Throughout these studies we used the Rudolf Research AutoEL-II ellipsometer to obtain the depth scales of the profiled specimens.

When the surface is opaque for visible light, and ellipsometry cannot be used, we employ local cross-sectional mechanical profiling. The general term of this approach is profilometry. The studied surface with non-uniformities on it is being moved beneath a diamond-tipped stylus attached to a piezoelectric sensor. Surface variations translating the stylus vertically are recorded with high precision as the scan progresses. In such a manner the cross-section of the SIMS crater can be restored and the SIMS data properly scaled. In our studies we used a Sloan profilometer, model "Dektak IIA".

Our group employs other relevant experimental methods, such as Atomic Force Microscopy and Rheometry. Their implementation in this part of the research effort was limited, and therefore we will leave off the detailed descriptions.

1.3. Sample preparation

For the purposes of an adequate SIMS experiment, the materials studied have to be specially prepared. Polymer samples are thin mono- or multilayered films deposited onto a very smooth surface of a substrate (predominantly a Si wafer).

To get a film with desired qualities, a standard sample preparation routine is employed. First, a wafer is cleaved into relatively small pieces (ca. 1 cm^2, to fit a SIMS sample holder). Originally, the surface is covered with a native oxide layer, as well as some other contaminants. This fact alone can have a dramatic effect on the physical and chemical properties of the surface. If we wish to alter the attributes of the surface it has to be chemically processed. Relevant etching procedures will be described below.

Polymers in a powder or granular state are dissolved in a solvent. Next, we spin cast our film from the polymer solution onto the surface of the wafer. The high rotation speed of a spinner spreads the droplet quickly as the solvent evaporates. As a result we have a smooth and rather uniform layer of the solute. The thickness of the layer obtained depends on many parameters, like concentration of polymer solution, time and speed of spinning, etc. Thus, we can easily adjust the desired thickness, which can be measured afterwards with an ellipsometer.

When preparing multilayered samples, spinning of the next film on top of the previous is usually not acceptable, since the solvent may destroy the interface between the two. Instead, the next layer is first spun on a piece of glass, and then floated in deionized water onto the lower coating. With many polymeric solutions this standard procedure works fine.

Often, a thermal treatment of the samples is required. They are placed inside an evacuated (pressure ca. 10^{-2} Pa) oven for various times at certain fixed temperatures in the range above the glass transition temperature and below the decomposition temperature for the given polymers. Parameters of annealing are crucial in many respects, which will be shown later. The TOF-SIMS instrument is designed with the built-in *in-situ* annealing feature significantly simplifying thermal processing of our specimens.

Finally, sometimes it is desirable to have an additional top sacrificial cover layer. SIMS sputtering process reaches equilibrium at a certain depth, giving ambiguous information about the initial phase of the run. For 2 keV bombardment, a 200 Å overlayer is adequate.

References

1. S. A. Schwarz, B. J. Wilkens, M. A. Pudensi, M. H. Rafailovich, J. Sokolov, X. Zhao, W. Zhao, X. Zheng, T. P. Russell, and R. A. L. Jones, *Mol. Phys.* **76**, p.937 (1992).

2. L. C. Feldman, J. W. Mayer, *Fundamentals of surface and thin film analysis*, Elsevier Science Publishing (1986).

CHAPTER 2

Polymers at interfaces

2.1. General properties of polymers

Polymers are materials made of molecules consisting of a large number of atoms usually arranged in chain-like structures. Polymer molecules also have the colloquial name 'macromolecules'. A group of atoms representing a primitive 'building block' of a macromolecule is called a monomer. Polymers can be characterized by their degree of poymerization N (the number of structural units in the chain), or, equivalently, by their molecular weight $M_w = N M_0$, where M_0 is the weight of a monomer. A distribution of molecular weights in a given state is referred to as polydispersity.

There is a significant diversity of macromolecule types as well as polymeric states. Polymer structures can be linear, star-like or comb-like (branched). The repeat units of a chain can be of a single type (e.g., -A-A-A-A-A-), or there can be several different types of monomers participating in formation of a macromolecule. In the first case the molecule formed is a homopolymer, in the second – a copolymer. If linear copolymer chains contain blocks of different monomers (e.g. -A-A-A-A-A-B-B-B-B-B-A-A-A-A-A-), they are called block copolymers. If blocks of one type (-B-B-B-B-B-) are grafted to a backbone of a different type (-A-A-A-A-A-) they are named graft copolymers. Also, there are other types of copolymers such as random (e.g., -A-B-B-B-A-A-B-A-A-B-A-) or

alternating (-A-B-A-B-A-B-A-).

Polymer materials usually have rather elaborate phase diagrams resulting from complex intra- and inter-molecular interactions. Giant polymer molecules form certain arrangements in three dimensions, which are called conformations. At low temperatures they can assemble themselves into regular (crystal) or random (glassy) structures. With increasing temperature, polymers may form random melts, where molecules are coiling and tend to float in a liquid-like manner, or liquid crystals with some alignment in a certain direction. Sometimes a gel phase results, when the chains cross-link with each other via chemical bonding, congregating into giant networks. One can also create polymer blends, consisting of two or more components of different polymer materials. Macromolecules can exist in a dilute state as well, when mixing a polymer with a certain solvent forms a solution. Depending on the nature of the solvent-monomer interaction, chains may either swell from their initial conformations or collapse on themselves.

In the case of a changeover from a viscous melt of polymer to its glassy state, one deals with the so-called glass transition. The characteristics and the type of this transition are still under debate, but it is possible to define rather unambiguously a glass transition temperature T_g at which apparent discontinuities appear in a specific heat.

The glass transition temperature is often very sensitive to many factors such as: molecular weight, polydispersity, chemical structure of a polymer, possible copolymerization, amount of cross-linking and crystallinity. There are alternative ways, thermodynamic as well as kinetic, of treating the glass transition temperature. One of the most important underlying ideas in this respect is the

concept of free volume, reflecting changes in configurational entropy of the chains. As the temperature is increased, the glassy polymer is expanding, creating extra room for molecules to move into, over and above the empty space of random close packing. At a certain point the chains have enough room for sustaining motion over distances comparable to the molecular sizes, and the material starts exhibiting viscous flow, when polymer molecules acquire enough thermal energy for tangible irreversible changes to occur in the bulk. If the chains don't cross-link into a rubbery network, we have an example of a typical polymer melt. The concept of free volume appeared to be very useful and was applied for the theoretical description of many processes in polymer melts and solutions.

Understanding the behavior of molecules in a melt has both fundamental and applied significance. One of the key parameters here is viscosity η, a physical quantity relating the shear stress to the strain rate. For classical (Newtonian) liquids, η is a constant, and the shear stress is linear with the strain rate. Polymeric melts, solutions, and networks very often exhibit strong deviations from the linear description, which gives rise to the term 'non-Newtonian liquids'.

The first empirical model relating viscosity and fractional free-volume was suggested by Doolittle [1], with

$$\ln \eta = a + \frac{bV}{V - V_0} .$$

Here a and b are constants. V and V_0 are respectively the real and occupied volumes at a given temperature. The concept of free volume was applied widely in

the rheology (theory of viscoelastic properties) of polymers originated by Williams, Landel, and Ferry [2] (the WLF theory). According to the WLF theory, the changes in liquid viscosity with frequency and temperature from T_g may be plotted on a single master curve by using the reduction factor $a_T = \eta_T/\eta_{Tg}$. The macroscopic rheological quantities such as viscosity can be derived from the models describing phenomena occurring on the microscopic scale. One of the first microscopic theories suggested was the Rouse-Beuche theory [3], [4]. Within it the polymer chain is modeled as a set of beads linked by springs. Each bead of the chain performs a random walk with constraints of self-avoidance. The friction between the chains and the environment modifies the motion and vibrations of the springs. The Langevin equations for the monomers can be rewritten in terms of normal coordinates $\mathbf{X}_p(t)$. Using the time correlation functions of the normal modes

$$R_p(t) = \frac{<\mathbf{X}_p(t)\cdot\mathbf{X}_p(0)>}{<X_p^2(0)>},$$

one can determine the relaxation modulus

$$G(t) = \frac{\rho k_B T}{N_b}\sum_p R_p(2t).$$

Where N_b is the number of beads and ρ is the monomer density. The viscosity then can be defined as

$$\eta = \int_0^\infty G(t)dt \ .$$

The notion of the radius of gyration R_g is introduced as the root-mean-square distance of chain segments from the center of mass of the coil:

$$R_g^2 = \frac{1}{N}\left\langle \sum_{i=1}^{N} (\mathbf{r}_i - \mathbf{r}_{cm})^2 \right\rangle .$$

It can be shown that the mean square end-to-end distance $\langle r^2 \rangle = 6\, R_g^2$. We can also introduce the mean square displacement of the center of mass

$$g(t) = \left\langle (\mathbf{r}_{cm}(t) - \mathbf{r}_{cm}(0))^2 \right\rangle .$$

Then the self-diffusion coefficient for a random walk of a chain can be defined as

$$D = \lim_{t \to \infty} \frac{g(t)}{6t} \ .$$

Based on those definitions, the Rouse-Beuche model brings forth the scaling dependencies for the viscosity $\eta \sim N$ and the diffusion coefficient $D \sim 1/N$. The function $g(t)$ scales linearly with t, providing time-independent values of the diffusion coefficient even for relatively short times. Interestingly enough, the bead-spring relaxation model was initially suggested for polymer solutions, but

numerous experiments confirmed its validity for a variety of polymer melts of relatively short chains. For the case of long chains however, a dramatic decrease in the scaling behavior is observed for both the viscosity $\eta \sim N^{3.4}$, and the diffusion coefficient $D \sim N^{-2}$. To explain these changes, a new scaling theory, known today as the reptation theory, was suggested by Doi and Edwards [5], and de Gennes [6].

The cornerstone feature of the new reptation model was an accounting of the effect of chain entanglements that was omitted in the Rouse-Beuche theory. It was dictated that for the case of long chains, passing of the molecules through one another is not allowed. As a result, the chains become trapped by the neighboring chains, creating a 'tube' of obstacles, allowing only for a reptile-like (thus 'reptation' !) motion in the tube. As a result, according to de Gennes, the scaling behavior is becoming significantly different. This approach allowed him to obtain an accurate result for the diffusion coefficient $D \sim N^{-2}$. As for the relationship between the melt viscosity and degree of polymerization, the predicted scaling power turned out to be slightly different from the one observed in experiments – 3 instead of 3.4. Later, corrections to the reptation picture (see, e.g. [7], [8], [9]) made it possible to elucidate the actual scaling behavior. For the motion of the center-of-mass, the reptation theory predicts two distinct scaling regimes: $g(t) \sim t^{1/2}$ for $t < \tau_R$ and $g(t) \sim t^{1}$ for $t > \tau_R$. Here $\tau_R \sim N^2$ is the time it takes for the chain to move a distance comparable to its size (reptation time).

It is also important to mention that the viscoelastic properties of polymers depend on the temperature. This issue, addressed by the WLF theory, has been examined extensively, and there exists a bulk of results for $\eta(T)$ and $D(T)$ dependencies in different regimes and for numerous systems.

Yet another significant aspect of polymer physics worth mentioning here is the behavior of polymer-polymer blends. Following Flory's thermodynamic approach [10], one can write the free energy for a uniform mix of two polymers A and B with degrees of polymerization N_A and N_B and the volume fractions ϕ and 1 - ϕ respectively:

$$\frac{F_b}{k_B T} = \frac{\phi}{N_A}\ln\phi + \frac{1-\phi}{N_B}\ln(1-\phi) + \chi\phi(1-\phi) \; .$$

Here the sum of the first two terms on the right hand side represents the entropic (combinatorial) contribution, while the third term is an enthalpy of mixing. The coefficient χ is usually referred to as the Flory-Huggins parameter. Since the volume fractions are less than one, the entropy part of the free energy is obviously negative, while χ for most simple hydrocarbon non-polar polymers is positive. For blends of polymers with high molecular weights, the enthalpy overpowers the first two terms (N_A and N_B are in the denominator, and the entropy is relatively small) and the free energy becomes positive, making a uniform mix unfavorable. As a result, the two components phase separate, and the blend becomes immiscible.

If a polymer has either block or graft copolymer parts that are not miscible with each other, the situation becomes more elaborate. The phase segregation may lead to a formation of a complex phase distribution, sometimes producing ordered structures with one-, two-, or three-dimensional periodicity.

2.2. Effects of the interface.

In any real system polymer materials are confined within certain boundaries. Those boundaries may represent interfaces with an ambient medium, solid surface, or other polymer. The presence of an interface affects, often dramatically, almost all the parameters of chain motion and conformation. Different factors and their combinations come into play, and we will discuss them briefly.

The first obvious contribution would come from the change in the free volume. At a solid surface, the motion of the chains will be restricted by the wall-like boundary and the molecules will have less room for flow. This can lead to the suppression of mobility, an increase in viscosity, and even local formation of a glassy phase. Effectively, a surface-induced modification of the glass transition temperature may occur. Another possibility would be the redistribution of degrees of freedom in highly anisotropic pancake-like macromolecular conformations. The geometric constraints may not be the only contribution to the altered interfacial polymer dynamics. The interaction energy between the monomers and the surface (solid, polymeric, or free) can render extra enthalpic contributions to the interfacial polymer properties. Several alternative mechanisms may affect viscoelastic macromolecular characteristics. If the surface is attractive (adsorbing) for the repeat units of polymer chains, it can lead to a decreased thermal expansion, producing in turn a reduction of the free volume. Chemical and physical interaction with the interface can effectively change the friction coefficient, employed in the Rouse and the reptation models. The vicinity of the surface may strongly affect formation of chain entanglements, crucial in view of the reptation properties. The presence of the interface also considerably affects the phase behavior in polymer

blends and mixtures. We will deliberate on this issue in the chapters to follow.

From the practical viewpoint, the behavior of polymers at solid surfaces strongly affects their wetting-dewetting properties, rheology, adhesion, and weatherability. The issue of interfacial dynamics of polymer chains is relatively new and still remains controversial in both fundamental and applied aspects, despite a substantial volume of the results obtained. Nonetheless, in the past several years, tangible progress has been achieved. A variety of experimental, theoretical, and computational techniques were employed in the effort to bring a unified view to the subject. There are still a few cornerstone questions which are not fully understood. In particular, in terms of polymer dynamics, what is the difference between a free surface and a solid interface, and for the latter, what is the contribution of such factors as attractiveness of the surface for the chains and pure geometric constrains? A brief review of some recent selected results here indicates that competing pictures have developed.

In 1990 Bruinsma [11] suggested a model in which polymer chain motion is strongly affected by the precursor region immediately at the surface. Later, Thompson, *et al.* [12] performed molecular dynamic simulations of thin films between two solid walls. Their results indicated formation of a wall-induced glassy phase with a substantial increase of the relaxation times. It was observed [13] that the substrate indeed affects the viscoelastic properties to a distance over several radii of gyration. The first direct ellipsometric measurement of the glass transition temperature was done in 1994 by Keddie, Jones, and Cory [14]. A decrease of the glass transition temperature was claimed. X-ray reflectivity experiments at NIST [15] focused on the thermal expansion of polystyrene films, with an increase in the

glass transition temperature observed. In [16], Forrest and co-workers were measuring T_g in free-standing films employing Brillouin light scattering. They argued that changes of the glass transition temperature at the free surface and at the substrate are interrelated in thin films, and depend on the combination of the polymer and the substrate. Another observation of increased T_g in ultra-thin films was recorded in [17] by X-ray reflectivity. The authors assumed an existence of a region with reduced chain mobility at the strongly favorable solid interface. Both substrate interactions and confinement effects were taken into consideration. Numerous additional studies in the previous decade have shown decreased mobility near the solid interface. In some cases, it has been suggested that entanglement effects result in long range inhibition of mobility. In 1993, AFM and X-ray diffuse scattering experiments [18] showed dewetting in thin polymer films that otherwise wet the surface at a higher annealing temperature, and a strong reduction of the diffusion coefficient was observed. SIMS depth profiling results [19], in 1995, indicated a reduction by two orders of magnitude of the diffusion coefficient at the polystyrene/SiO interface, attributed to a monomer-surface friction mechanism. Bychuk and O'Shaughnessy [20], predicted anomalous surface diffusion for the systems with an imbalance of readsorption and desorption times. Khare, *et al.* [21] employed molecular dynamics simulations for the case of confined polymer melts in a shear flow. They obtained an increase in viscosity with the decreased film thickness. (A similar result was obtained by Semenov [22]). They also observed stretching and alignment of the chains in the direction of the shear. Frank, *et al.* [23] measured a decrease in the lateral diffusion of dye-labeled chains using a fluorescence recovery technique, and discussed a molecular weight dependence for

the dynamic properties of polymer melts. X-ray absorption spectroscopy measurements on polystyrene [24] did not show mobility variations at the free surface. In a similar study, Lin, Wu, and Satija [25], employing neutron reflectometry, found a strong dependence of the diffusion coefficient on the distance form the solid wall extending over several radii of gyration. They assumed a strong interdependence of distorted chain conformations and the substrate interaction energy. Similar results [26] were obtained for the diffusion coefficient in a tri-layer system, as discussed below. Jones and co-authors [27] performed small angle neutron scattering experiments on a mixture of polystyrene and deuterated polystyrene, and found that chains retain their bulk conformations even with very strong confinement present.

Thus, in view of the novelty of the problem of interfacial polymer behavior as well as the unsettled classification of the results, we pursued further studies in this area. Understanding the main features of that subject is very meaningful from both fundamental and practical viewpoints. The aim, obviously, is the ability to predict interfacial properties and to generalize them for miscellaneous systems, and each new experimental approach brings us closer to that goal.

References

1. A. Doolittle, *J. Appl. Phys.* **22**, p.1471 (1951).
2. M. J. Williams, R.F. Landel, I.W. Ferry, *Amer. Chem. Soc.* 77, p.4701 (1955).
3. P. E. Rouse, *J. Chem. Phys.* **21**, p.1272 (1953).
4. F. Bueche, *J. Chem. Phys.* **22**, p.603 (1954).
5. M. Doi and S. F. Edwards, *The Theory of Polymer Dynamics* (Clarendon Press,

Oxford,1986).

6. P. G. de Gennes, *Scaling Concepts in Polymer Physics* (Cornell University Press, Ithaca, 1979).
7. J. M. Deutsch, *Phys. Rev. Lett.* **54**, p.56 (1985).
8. A. N. Semenov, *Physisa A.* **166**, p.263 (1990).
9. M. Rubinstein and S. P. Obukhov, *Phys. Rev. Lett.* **71**, p.1856 (1993).
10. P. Flory, *Principles of Polymer Chemistry* (Cornell University Press, Ithaca, 1971).
11. R. Bruinsma, *Macromolecules* **23**, p.276 (1990).
12. P. A. Thompson, G. S. Grest, and M. O. Robbins, *Phys. Rev. Lett.* **68**, p.3448 (1992).
13. H.-W. Hu and S. Granick, *Science* **258**, p.1339 (1992).
14. J. L. Keddie, R. A. L. Jones, and R. A. Cory, *Europhys. Lett.* **27**, p.59 (1994).
15. W. E. Wallace, J. H. van Zanten, and W. L. Wu, *Phys. Rev. E* **52**, p.R3329 (1995).
16. J. A. Forrest, K. Dalnoki-Veres, J. R. Stevens, and J. R. Dutcher, *Phys. Rev. Lett.* **77**, p.2002 (1996).
17. J. H. van Zanten, W. E. Wallace, and W. L. Wu, *Phys. Rev. E* **53**, p.R2053 (1996).
18. W. Zhao, M. H. Rafailovich, J. Sokolov, L. J. Fetters, R. Plano, M. K. Sanyal, S. K. Sinha, and B. B. Sauer, *Phys. Rev. Lett.* **70**, p.1453 (1993).
19. X. Zheng, B. B Sauer, J. G. Van Alsten, S. A. Schwarz, M. H. Rafailovich, J. Sokolov, and M. Rubinstein, *Phys. Rev. Lett.* **74**, p.407 (1995).
20. O. V. Bychuk and B. O'Shaughnessy, *Phys. Rev. Lett.* **74**, p.1795 (1995).

21. R. Khare, J. J. De Pablo, and A. Yethiraj, *Macromolecules* **29**, p.7910 (1996).

22. A. N. Semenov, *Phys. Rev. Lett.* **80**, p.1908 (1998).

23. B. Frank, A. P. Gast, T. P. Russell, H. R. Brown, and C. Hawker, *Macromolecules* **29**, p.6531 (1996).

24. Y. Liu, T. P. Russell, M. G. Samant, J. Strohr, H. R. Brown, A. Cossy-Favre, and J. Diaz, *Macromolecules* **30**, p.7768 (1997).

25. E. K. Lin, W.-l Wu, and S. K. Satija, *Macromolecules* **30**, p.7224 (1997).

26. X. Zheng, M. H. Rafailovich, J. Sokolov, Y. Strzhemechny, S. A. Schwarz, B. B. Sauer, and M. Rubinstein, *Phys. Rev. Lett.* **79**, p.241 (1997).

27. R. L. Jones, S. K. Kumar, D. L. Ho, R. M. Briber, and T. P. Russell, *Nature* **400**, p.146 (1999).

CHAPTER 3

Depth and time dependence of polystyrene chain diffusion near a solid interface

In this chapter we present original results on interfacial polymer dynamics, reported in [1] and [2]. The material we investigate is polystyrene (PS), a common polymer employed in numerous studies. PS has a monomer unit of the following composition:

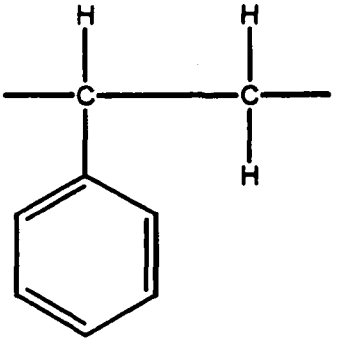

In order to elucidate the dynamic behavior of PS chains we prepare polymer samples consisting of multiple layers. Some layers are made of deuterated polystyrene (dPS), where all hydrogen atoms are replaced by deuterium. The details of the sample preparation technique are described in Chapter 1. The samples are annealed above the glass transition temperature, which allows the macromolecular chains to flow viscously, and the layers of the samples may interdiffuse as a result. The specimens are cooled back to temperatures below T_g

and subjected to SIMS depth profiling (see Chapter 1). Isotopic tagging in dPS makes it possible to visualize, upon heating, the rates of diffusion in the direction normal to the sample surface. The described technique was first employed about a decade ago (see for example [3], [4], [5]), and is accepted now as one of the direct ways of measuring the diffusion coefficient in polymers.

A primary goal of this part of our research is to get a better understanding of the phenomena occurring in polymer melts in the presence of a solid interface. The discussion in the previous chapter brings up the question of what is the impact of the substrate (as well as any other interface) and its conditions on the dynamics of polymer chains. Analysis of the current state of affairs in this field given in Chapter 2 indicates that the dynamics of macromolecules in the vicinity of a solid surface is significantly altered, and there may be several mechanisms responsible for this modification. Prior to the present studies, the topic had been addressed increasingly in the last couple of years. Many important results have been contributed by the current participants of the Garcia Center, as well as by a number of other groups. These findings strongly favor the picture in which polymer chain diffusion is significantly inhibited due to the presence of the wall.

In [6], the diffusion coefficient was measured in a thin film PS/dPS system in the vicinity of several different interfaces: native oxide covered silicon, a silicon surface hydrogen passivated via HF etching (see Chapter 4 for details), a silicon surface covered with a very thin layer of polyvinylpyridine (immiscible with PS), and the vacuum interface. The SiO and SiH surfaces revealed a dramatic (two orders of magnitude) suppression of diffusion compared to the bulk values. The polyvinylpyridine (PVP) surface, an almost "non-sticky" interface, yielded a

decrease of D by less than an order of magnitude, while at the vacuum surface the behavior was very close to bulk-like. The authors speculated that the results observed could be explained by the nature of polymer-surface interaction – strong for the case of SiO and SiH surfaces and weak at the PVP interface. Although the mechanism of diffusion inhibition is complicated, it can be treated within certain model approximations. If we treat the surface as a "sticky" plane, then for the friction of the reptating chains one must account for the effect of polymer-surface interaction. It was suggested that the reduction in diffusion rates at the solid wall could be attributed to the modified friction force in a simple generalization of the reptation model, in which the diffusion coefficient at the surface is scaling with the degree of polymerization as $D \sim N^{-3/2}$. It was shown that in the immediate vicinity of the attractive silicon interface, polystyrene diffusion has the predicted scaling behavior with the molecular weight. Thus, the correction of the friction force is a reasonable "first-order" approach. Nonetheless, all the depth profiles obtained in [6] reveal a common feature that can not be explained within a modified friction model. The diffusion tails of the tracer components outspread far beyond the distances that correspond to the radius of gyration R_g for the species of interest.

To explain this result within an adequate mechanism of long-range effects, an additional set of thin multilayer polymer films on a silicon substrate has been prepared in [7] for dynamic SIMS depth profiling. A dPS layer was sandwiched between two PS layers. The molecular weight (M_w) of dPS was 90K, while M_w of the matrix PS was 770K. The distance of the marker layer from the silicon native oxide surface was varied from 80 Å to 1880 Å, providing a procedure to measure D as a function of a distance from a solid wall. The thickness of the dPS marker layer

was the same for all the samples - ca.130 Å. The samples were annealed in vacuum at 153°C for times ranging from 10 minutes to 2 hours. The SIMS depth profiles of deuterium for 90K dPS in a matrix of 770K PS (R_g = 235 Å) are shown in Fig. 3.1. The experimental profiles were fitted with two different diffusion constants for the SiO- and vacuum- side slopes of the concentration profiles. Figure 3.2 shows averages of the two as a function of the distance from the SiO surface. The plots clearly indicate that the diffusion is dramatically slowed down out to X_w > 1000 Å, more than 10 R_g of the 90K dPS (R_g = 78 Å). D is scaling approximately as a 3/2 power of distance from the wall, a straightforward demonstration that PS diffusion is strongly inhibited over a distance of several times the radius of gyration from an attractive silicon surface. Annealing times were selected so that the deuterated chains did not physically contact the SiO surface. As can be seen, the deuterium profiles have not reached the substrate and, therefore, there is no direct contact of the dPS with the wall that could inhibit the diffusion. If we exclude a direct effect of the interface, the matrix polymer mediation must be a major mechanism of diffusant-surface interaction. It was concluded that the inhibition of diffusion could be due to entanglement buildup effects near the attractive interface, or to an increase in the local glass transition temperature.

In a different study [8], a significant modification for the time scaling of the diffusion coefficient at the solid interface was observed on a similar system. In PS/dPS bi-layer samples, the spread of the interface was measured as a function of the annealing time. It was found that the $t^{1/2}$ power dependence of $g(t)$ (see Chapter 2) extends over times significantly greater than the reptation time.

We need to point out that the diffusion coefficients calculated in [6] and

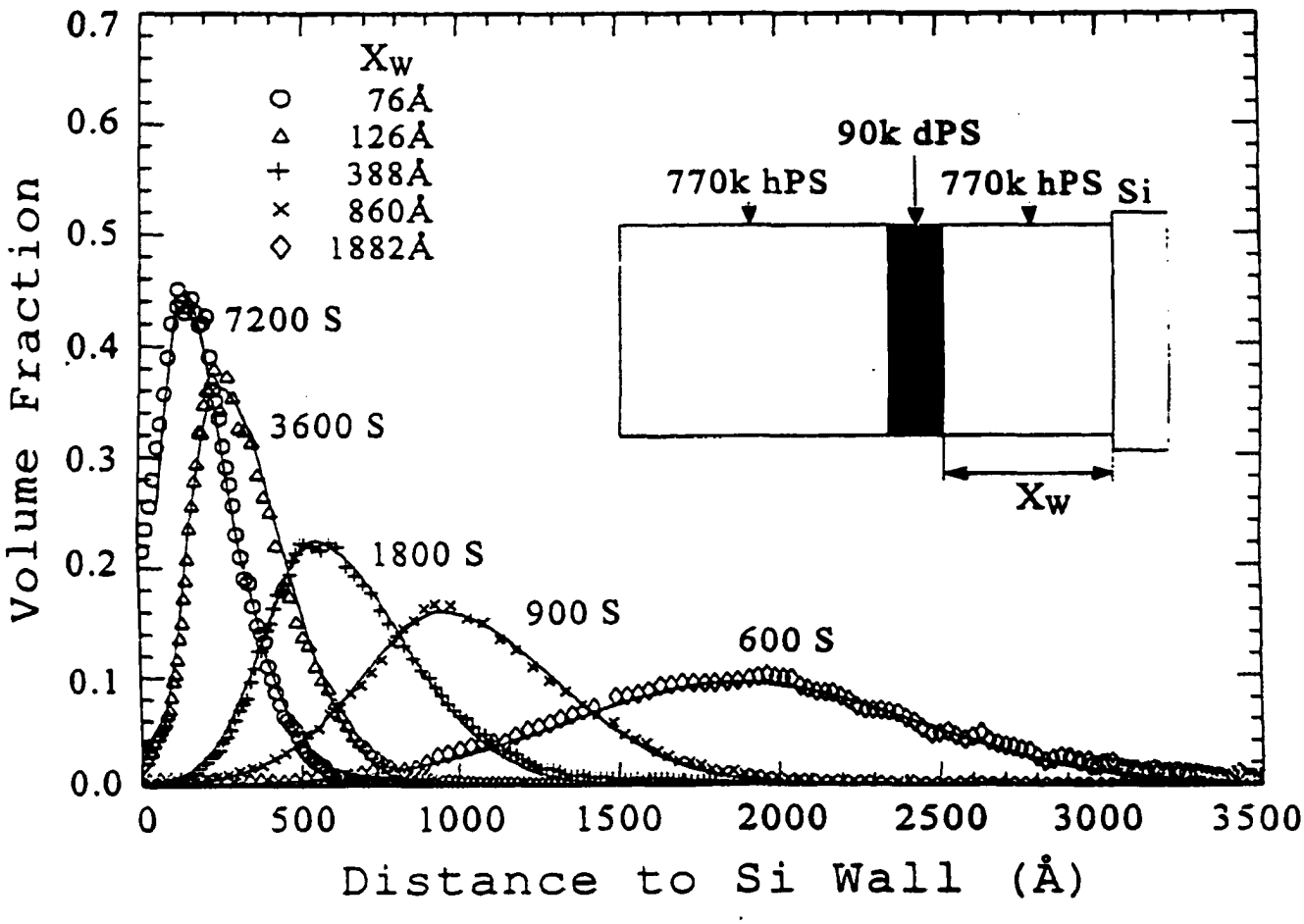

Figure 3.1 Profiles of dPS volume fraction vs. distance for the (770K PS/90K dPS/770K PS) sandwiches annealed at 153°C for times from 10 min. to 2 hrs. Curves are diffusion calculations to fit the slopes on either side of each peak with a single average diffusion constant. The variable geometry of the samples is shown in the inset [7].

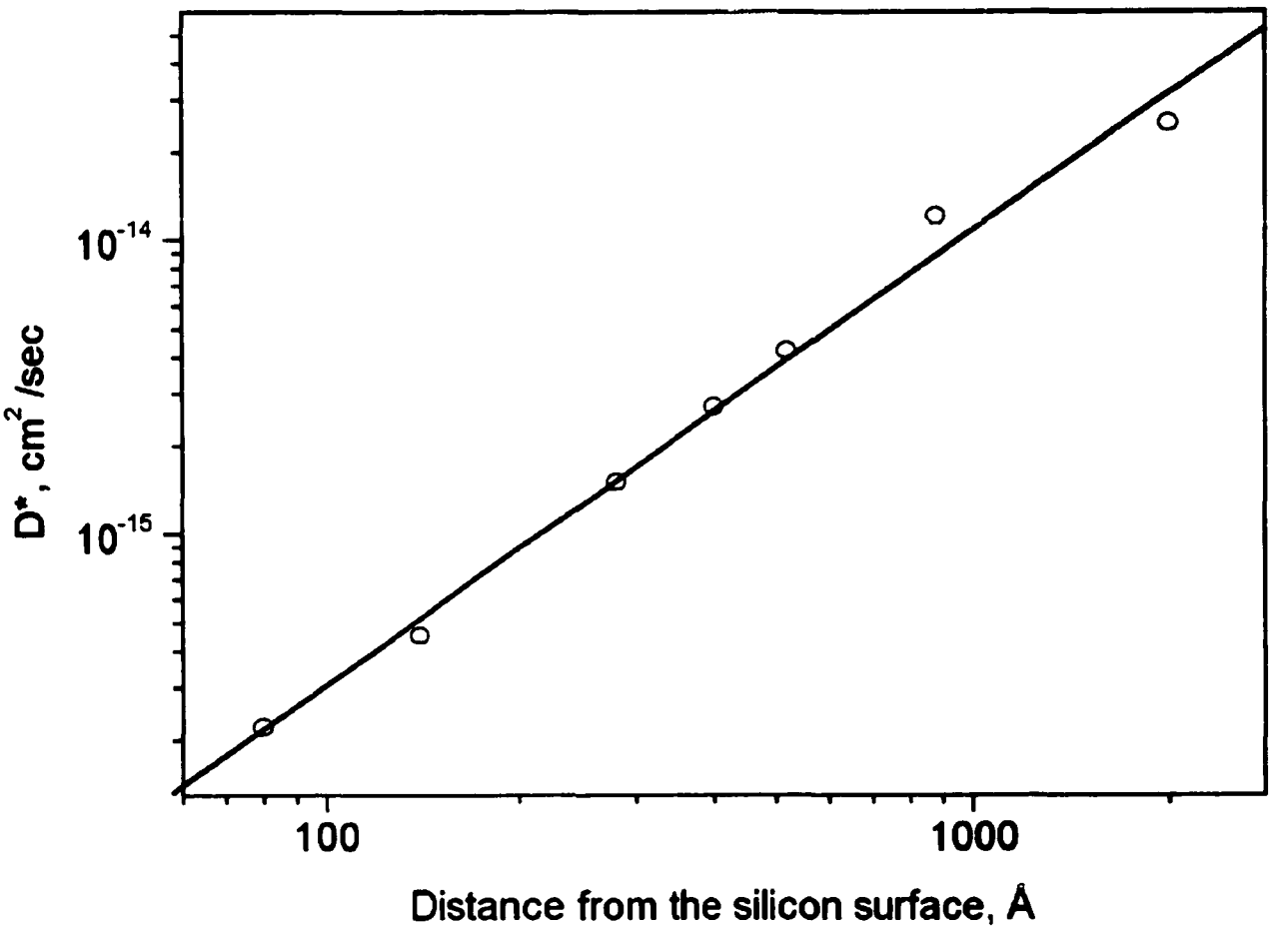

Figure 3.2 Values of the average diffusion constants, fitted to the tails of the profiles of Fig. 3.1, indicate that D rises with roughly a 3/2 power depth dependence with distance from the silicon surface.

[7] assumed no time dependence, while the ones calculated in [8] assumed no depth dependence.

It was logical to extend the studies of [6], [7], and [8] to other molecular weights and temperatures. But the most important question we planned to address was *whether the polymer chain dynamics could reveal a nontrivial time and space dependence simultaneously.*

In [1], we prepared 10 identical tri-layer polymer sandwiches. The bottom 280 Å-thick 670K PS layer was spin-cast from a toluene solution onto an unstripped Si (100) wafer. The subsequent layers of 150Å-thick marker 947K dPS and 860 Å-thick matrix 670K PS were floated in deionized water onto the sample surface. Nine samples were annealed separately in vacuum at 157°C for 2, 3, 6, 7.25, 10, 13.5, 22, 25, and 43 hours. The order of these anneals was random. To observe the time variation of the concentration, a quadrupole "ATOMIKA" SIMS instrument was employed. The primary argon ion beam had an energy of 2 keV with 30° off-normal incidence. All the samples upon annealing were covered with a thin protective PS overlayer, allowing steady-state behavior to be obtained in the SIMS depth profile before reaching the tri-layer body. Negative ions of the following species were monitored: F, D, C, CH, CD, O, Si, and CN. Depth profiles of deuterium, complemented by their CD and CH counterparts, were used to characterize the redistribution of polymer chains initially contained in the middle dPS layer. The signals of F, C, O, Si, and CN were used to obtain reliable information about the exact position of the interfaces between the polymer layers, as well as the polymer-solid and polymer-vacuum boundaries. The deuterium profiles were normalized to the carbon signal profiles, to correct for minor

variations of the sputtering yield due to charging or other instrumental artifacts. The run-time axis was converted to depth using the fluorine interfacial peaks as tags. The concentration scale was determined by integrating over depth, assuming mass conservation. A relatively small background, as determined in the PS overlayer, was subtracted to account for both a natural D/H isotope abundance and a possible H_2 ion interference.

These processed deuterium data are shown in Fig. 3.3. It is clear that along with a strong diffusion behavior, one can observe segregation of the deuterated component developing in time at the SiO interface, and later at the vacuum interface.

Surface segregation in the PS/dPS blends is a well-known effect, and it occurs as a result of a difference between surface energies of PS and dPS. There are several alternative models describing this phenomenon, but one of the most viable was developed in [9], [10], and [11]. Within a generalization of the Flory thermodynamic approach (see Chapter 2) it was shown that the thermodynamic potential of the system unit area is

$$\frac{F[\phi(x)]}{k_B T} = \int_0^\infty dz \left[\frac{F_b}{k_B T} - \Delta\mu\phi + \frac{a^2}{36\phi(1-\phi)} \left(\frac{d\phi}{dx} \right)^2 \right] + \frac{F_s}{k_B T}$$

Here F_b is the bulk free energy density, described in the previous chapter, $\Delta\mu$ is the exchange chemical potential, a, a segmental length, and F_s is a bare surface energy. Variation of the thermodynamic potential vs.ϕ in the linear approximation yields an

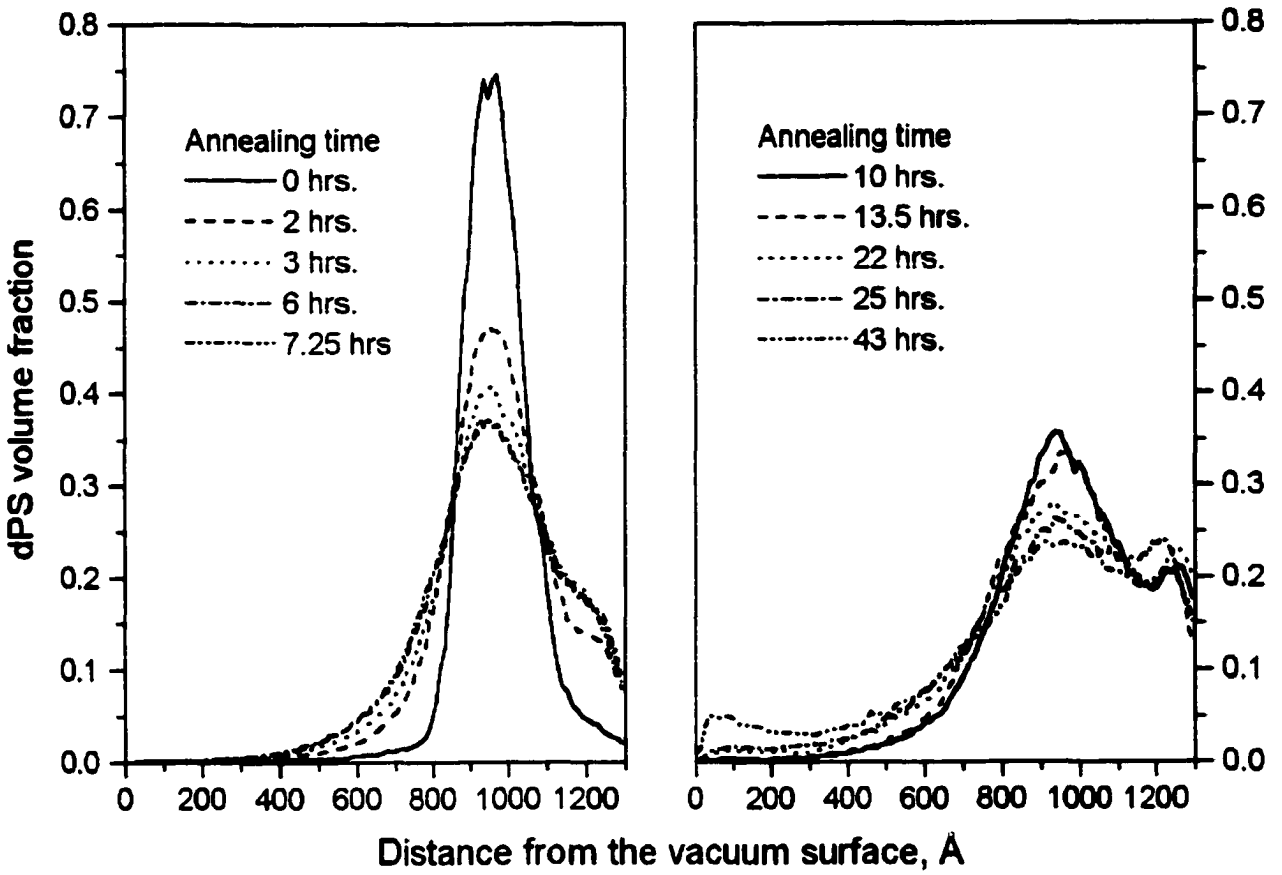

Figure 3.3 The left plot shows the normalized SIMS concentration profiles for an unannealed PS(280 Å, 670K)/dPS(150Å, 947K)/PS(860 Å, 670K) sandwich structure, and for samples annealed at 157°C in vacuum for 2, 3, 6, and 7.25 hours. The right plot shows the same sample following anneals of 10, 13.5, 22, 25, and 43 hours.

exponential $\phi(x)$ dependence.

In order to elucidate the behavior of the PS diffusion, we employ a model based on a one-dimensional continuity equation linear in dPS relative concentration $\phi(x,t)$:

$$\frac{\partial \phi(x,t)}{\partial t} = -\frac{\partial J(x,t)}{\partial x}$$

with impenetrable walls for the boundary conditions (i.e., $J(x_t,t) = 0$). The total flux $J(x,t)$ involves both the diffusion and the segregation components:

$$J(x,t) = -D(x,t)\left[\frac{\partial \phi(x,t)}{\partial x} + \frac{1}{l}\left(\phi(x_t,t) - kz^*\right)e^{-\frac{(x-x_t)}{l}}\right].$$

Here l is the correlation length of segregation; k is the desorption parameter; x_t is the total thickness of the sandwich sample, and z^* is the surface excess determined (similar to [11]) by:

$$z^* = \int_{x_0}^{x_t}\left[\phi(x,t) - \phi(x_0,t)\right]dx; \qquad \frac{\partial^2 \phi}{\partial x^2}(x = x_0) = 0$$

This set of equations has a stationary solution:

$$\phi(x) = A + Be^{-\frac{x_t - x}{l}}; \qquad A, B = const,$$

which is consistent with the predictions of [9] – [11]. In these equations, segregation at the $x = x_f$ boundary is controlled by the concentration at the boundary $\phi(x_f, t)$ and desorption is controlled by the surface excess z^* and rate k. The values of l and k are held constant at 70 Å and 0.14 $Å^{-1}$ respectively, similar to the values employed in [11], and providing a reasonable fit to the current data. Although present in the experimental output, the vacuum surface segregation is neglected in our equations due to its relative insignificance. We exclude it from the calculations also to avoid the introduction of an extra fitting parameter. An important feature of our approach is the fact that the diffusion coefficient D is allowed to vary with both depth and time.

Based on the proposed model, a computer program was designed generating libraries of concentration profiles for different numbers of iteration cycles and varying assumptions for the depth dependence of the dimensionless diffusion coefficient $d(x)$. To account for the experimental SIMS broadening the generated profiles were convolved with a Gaussian. The width of the Gaussian (FWHM) was determined from the fit for the unannealed sample. The program then calculated average-square deviations between the ten SIMS profiles and the convolved data from the numerical simulations. A typical plot for the sets of fitting curves is shown in Figure 3.4.

The first tested model was a constant uniform $d(x)$. The results of the best fit for the sample annealed for 7 hrs. is shown in Fig. 3.5(a), while the best fit for the 22 hr. anneal is shown in Fig. 3.5(d). The SIMS profile is superimposed with the original and the convolved library profiles. It is evident that at 22 hours, the

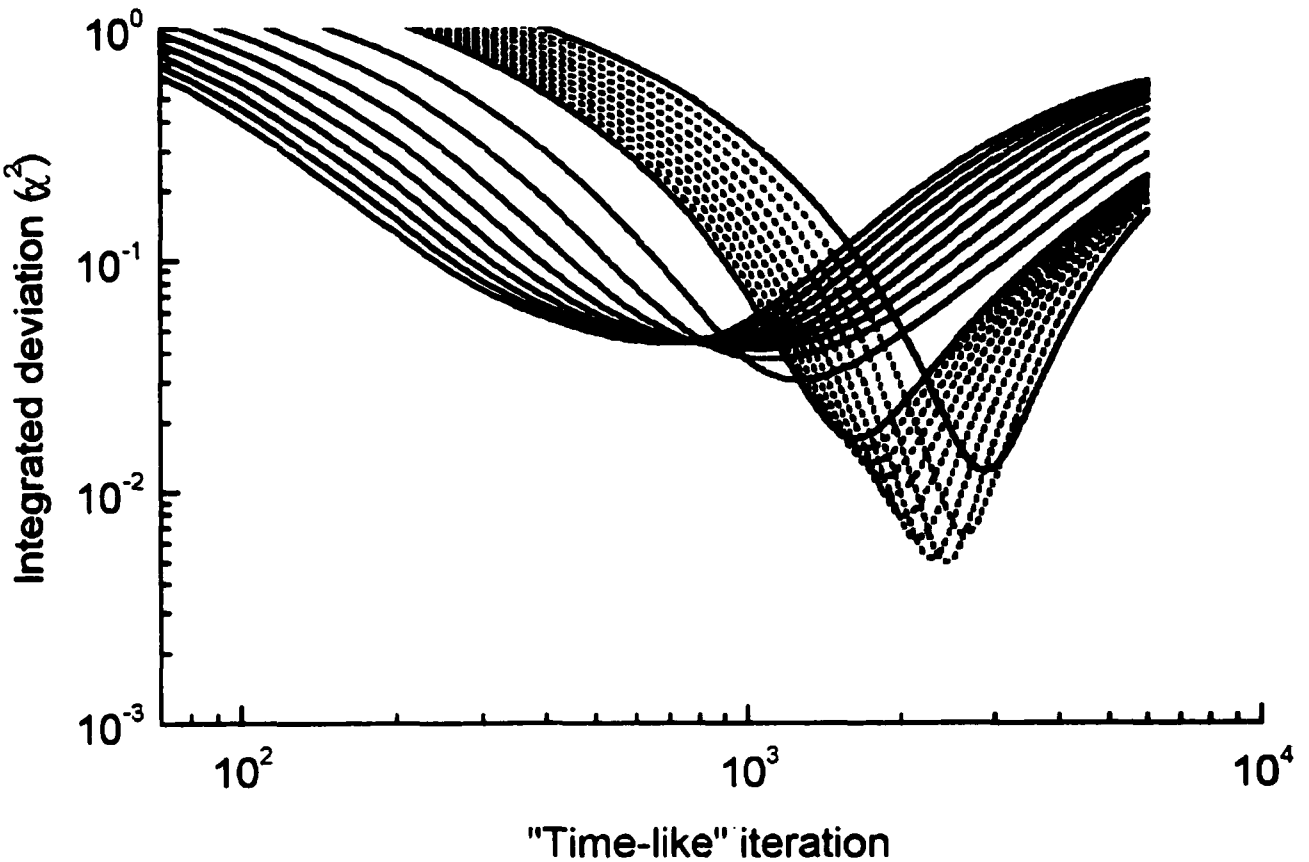

Figure 3.4 An example of a set of curves for detecting the best integrated deviation (χ^2). The deviations are obtained between a certain experimental SIMS profile and a set of computer-generated convolved 'library' curves for variable assumptions of *d(x)*. The minimum is sought as a function of the number of 'time-like' steps in the algorithm. The minimum corresponds to the least square fit for a given annealing time.

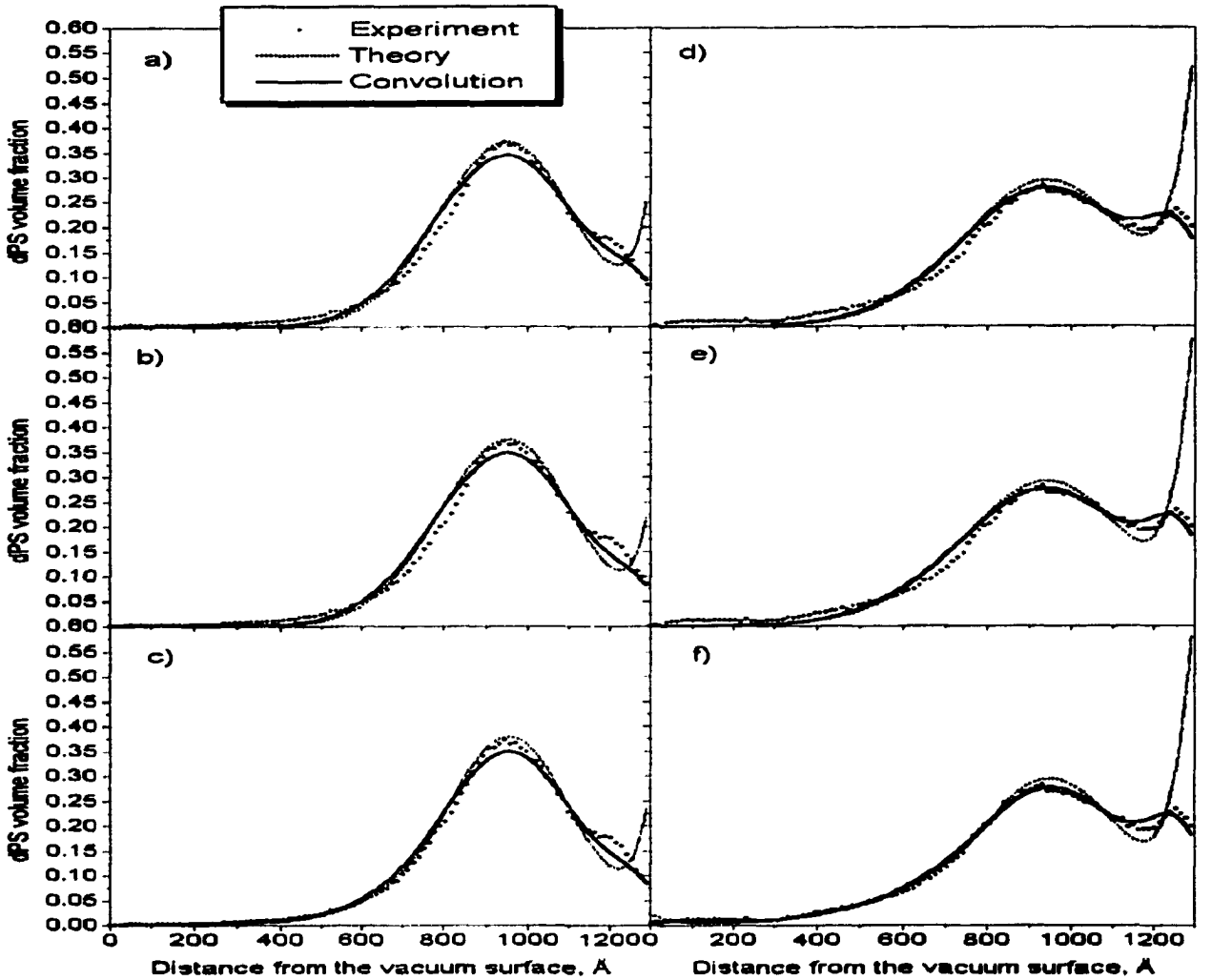

Figure 3.5 The experimental SIMS profiles (dotted) for anneals of 7 hrs. (left plots) and 22 hrs. (right plots) are contrasted to the numerical predictions before (dashed), and after (solid), the gaussian convolution which mimics SIMS induced broadening. The top plots (a) and (d) are for the assumption of a constant *d(x)* with depth. A *d(x)* rising linearly toward the vacuum interface improves the fit at long times (e) but degrades the fit at short times (b). A two piece linear fit, (c) and (f), markedly improves the quality of the fit at long and short annealing times in all samples.

long tail extending into the bulk towards the vacuum surface is not fit well by the theoretical curve. (This feature is reproduced for all the SIMS samples annealed at longer times). This is an indication of a non-uniform diffusion behavior. It is natural that the next tested *d(x)* vs. *x* behavior was a linear increase away from the wall with a variable slope. The best-fit results for the 7 hr. and 22 hr. samples are presented in Figures 3.5(b) and 3.5(e) respectively, where *d(x)* increases by a factor of 1.5 between the SiO and vacuum interfaces. For greater slopes the computer-generated profiles acquire significant asymmetry in the vicinity of the deuterium concentration peak, and the quality of the fits deteriorates, especially for the short time anneals.

In order to account for the symmetric shape of the profile near the deuterium concentration peak and the extending concentration tails in the bulk, we employed a two-piece linear dependence for *d(x)* consisting of a constant value within 400 Å of the wall, and then rising linearly in value toward the vacuum interface at various rates. Figures 3.5(c) and 3.5(f) show the best fits obtained. The quality of the fit for these and all other samples is improved substantially. The ratio of the *d(x)* values near the vacuum and the SiO surfaces for the best fit is approximately 5.5.

For all the tested models, we determined the value of the time-like iteration cycle-number for the best fits. These values are plotted in Fig. 3.6 as a function of the annealing time, for the three models (constant, linear, and two-piece) employed in Fig. 3.5. Assuming stationary diffusion, one would have expected a linear dependence of computer time on annealing time. Instead, a very strong non-linear dependence was observed, scaling with annealing time

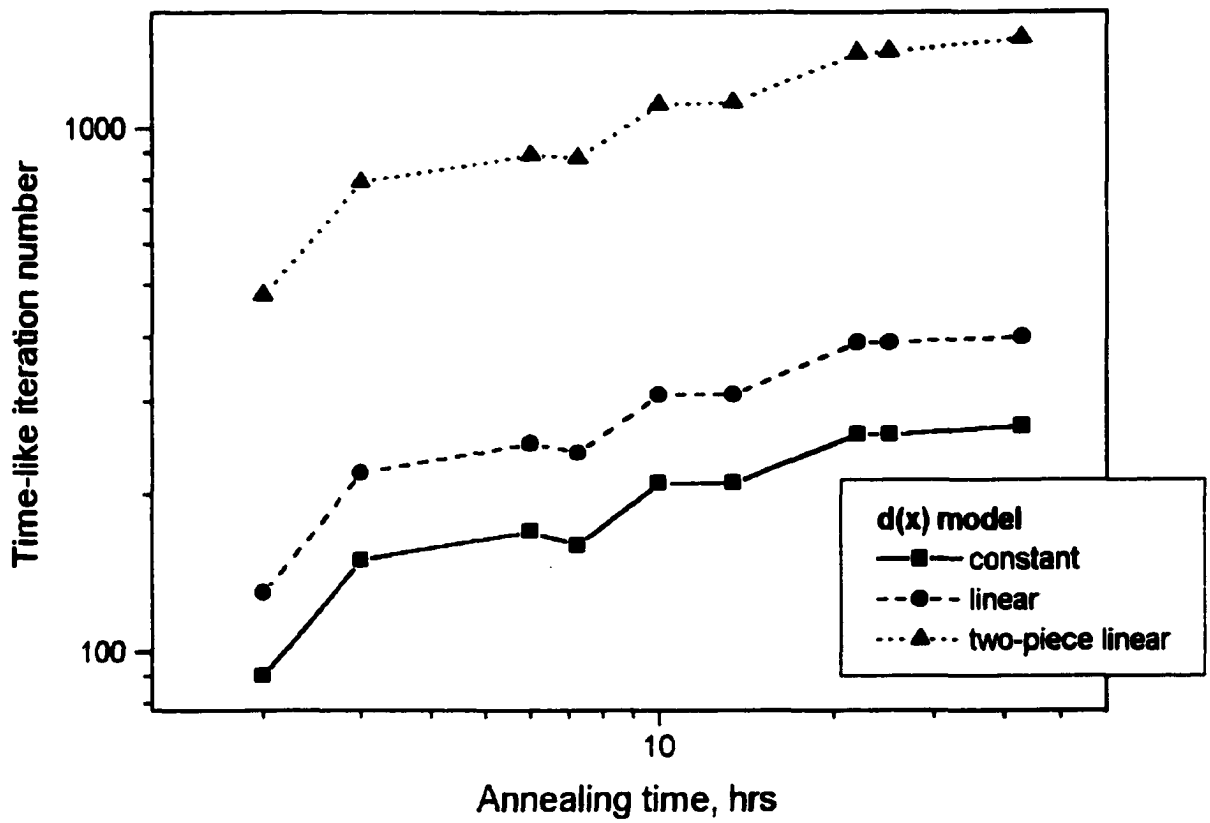

Figure 3.6 The number of time-like iteration cycles producing best fits in the constant (solid), linear (dashed), and two-piece (dotted) models are plotted vs. the actual annealing time.

approximately as a power of 1/3 in all cases. The time dependence was also found to be relatively insensitive to the magnitude of the linear slopes employed. We concluded that this is a robust indication of a time-dependent inhibition of PS chain diffusion in this system.

For the molecular weights and the annealing temperature employed, the bulk value of D predicted in [12] is approximately 6×10^{-16} cm^2/sec. The values of D in our best fits are everywhere less than this value. For the case of a constant diffusion illustrated in Figures 3.5(a) and 3.5(d), the values of D are 5.1×10^{-17} cm^2/sec. at 7 hrs. and 2.55×10^{-17} cm^2/sec. at 22 hrs. These values are, of course, predicated on the assumption that D does not change as the concentration profile develops in time.

Evidently, the system examined demonstrates that the depth dependence of the diffusion coefficient should be super-linear, i.e., varying slowly near the SiO interface and rising more rapidly toward the vacuum interface, and that the diffusion coefficient in the vicinity of the marker layer must decrease with time within many hours of annealing.

Nonetheless, certain difficulties were encountered in analyzing the results quantitatively. Because of the strong preferential surface segregation of the deuterated species, an extra number of fitting parameters had to be dealt with, degrading the quality of the fits. Also, due to the PS/dPS molecular mass mismatch, the diffusion coefficient becomes a nonlinear function of the volume fraction [13], and the analysis becomes more complex.

In conjunction with this, it was reasonable to reduce the experimental and computational error by matching the molecular weights of PS and dPS, and, more

importantly, employing for a substrate surface a substance with strong attractive properties yet capable to suppress the preferential segregation. Recently, Zhang, *et al.* [14] have observed a suppression of diffusion throughout a carbon-black composite, suggesting that the surface of the filler particles may induce a local inhibition of diffusion. At the same time, a non-polar nature of carbon should not favor dPS over PS in a blend. These considerations have determined our choice of the alternative for the native oxide as a solid wall.

In [2], we prepared a set of identical tri-layer polymer samples on two different solid surfaces: native silicon oxide and a carbon film sputter-deposited on a silicon wafer. The thickness of the carbon film was approximately 100 nm. These sandwiches had the following structure: PS(980Å)/dPS(150Å)/PS(200Å)/[C]/Si. Molecular weights of PS and dPS were chosen to match each other closely (Polymer Source, Inc., 670K, R_g=215 Å and 690K, R_g=220 Å, respectively). The bottom PS layer was spin cast from a toluene solution, and the top layers were floated in deionized water. The samples were annealed at 157°C in vacuum for 1, 2, 3, 5.5, 7, 15, 20.25, 22, and 46 hours. The sequence of these anneals was chosen at random, and each time the counterparts on the two different surfaces were annealed simultaneously. All samples were subject to SIMS depth profiling on the "ATOMIKA" instrument. The method of data conversion was similar to the one described above. The obtained SIMS depth profiles of the deuterium signals are shown in Fig. 3.7. One can see a significant difference in the profile evolution between the two surfaces. On the Si surface, during the first seven hours of annealing time, the diffusion and Si-surface segregation are unfolding simultaneously, while after seven hours, the chain distribution reaches a

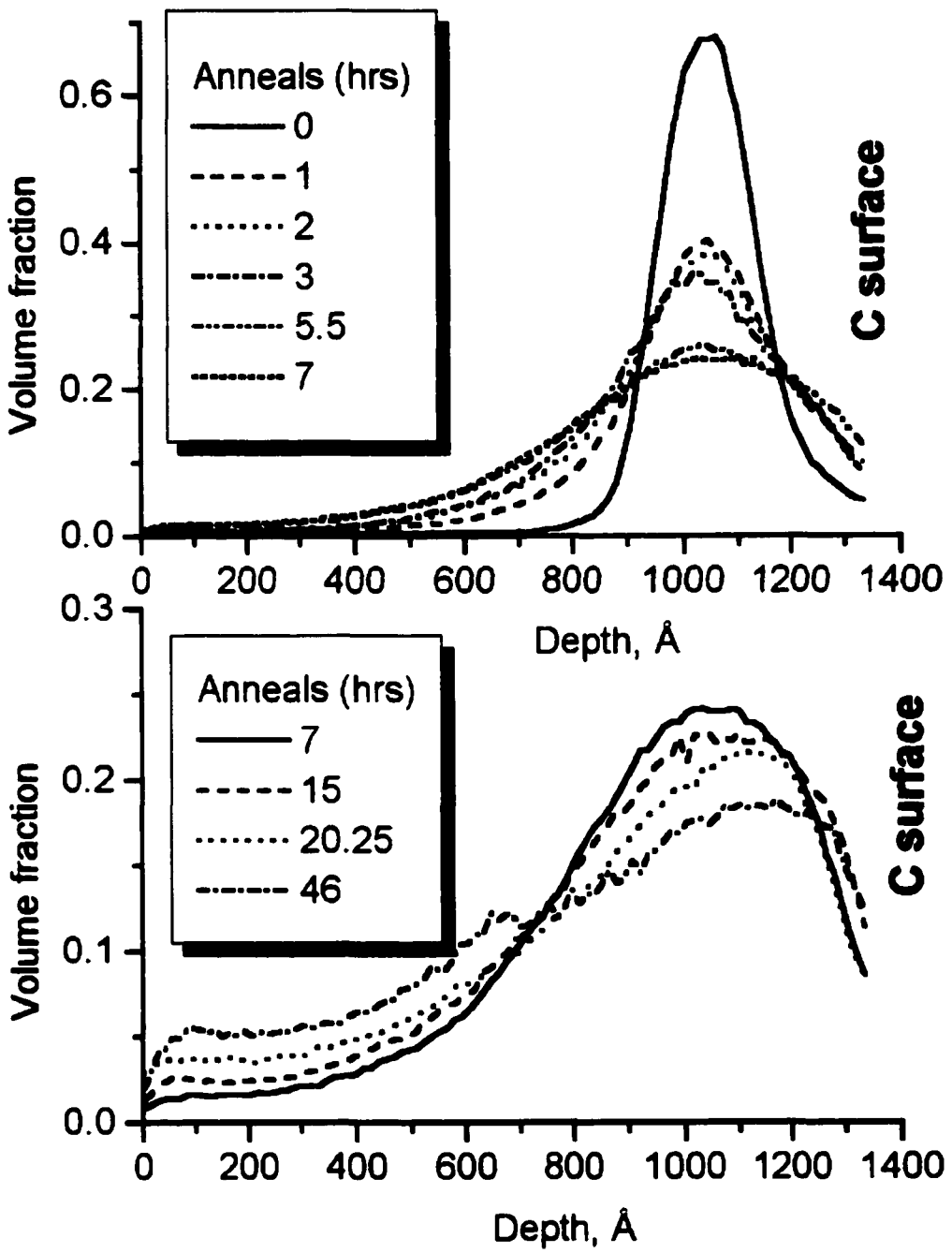

Figure 3.7.a The plot shows the normalized SIMS concentration profiles for the PS(980Å, 670K)/dPS(150Å, 690K)/PS(200Å, 690K) sandwich structure on the carbon surface, annealed at 157°C in vacuum for 0, 1, 2, 3, 5.5, 7, 15, 20.25, and 46 hours.

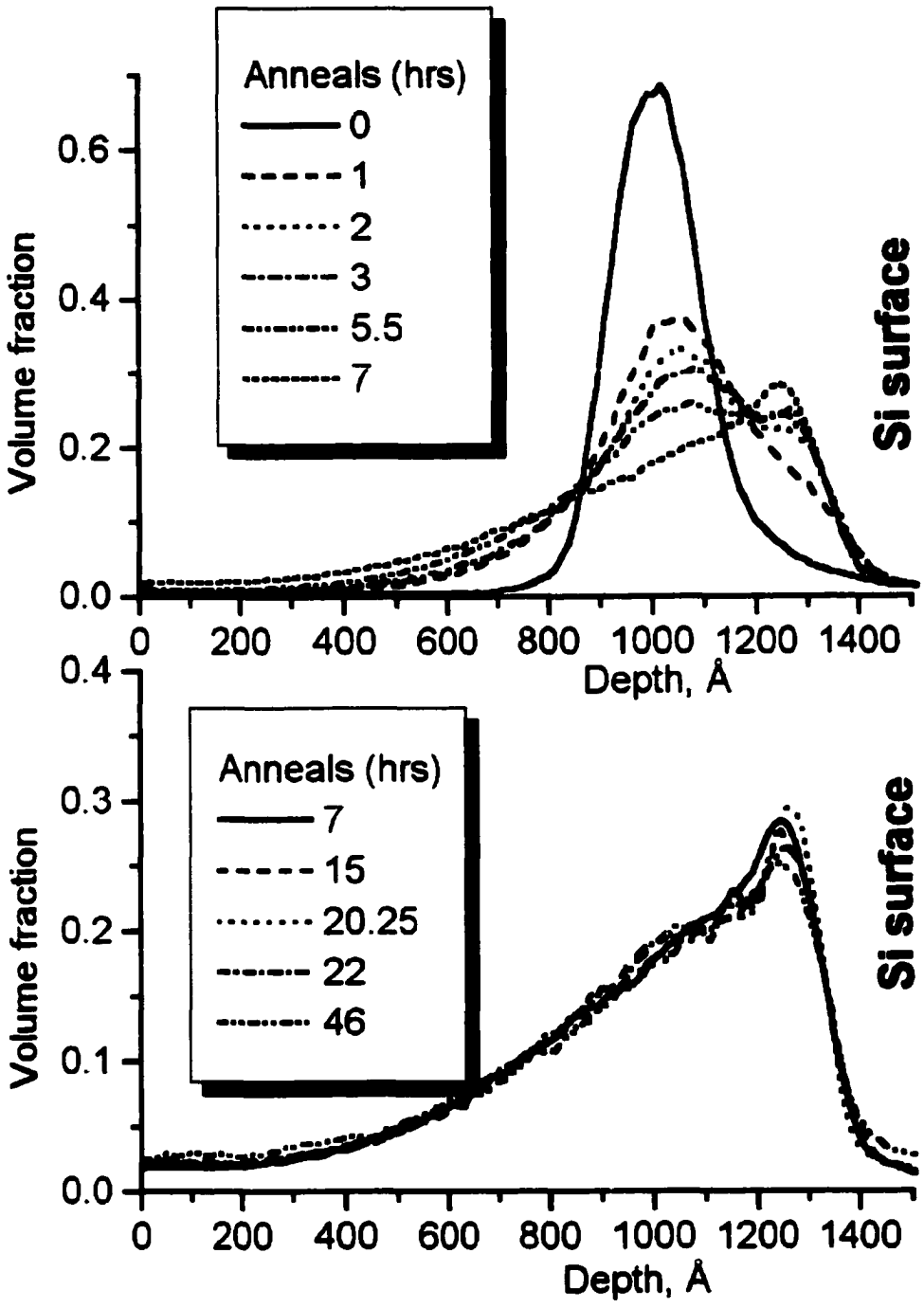

Figure 3.7.b Concentration profiles for the same sandwich structure on a native Si surface following anneals of 0, 1, 2, 3, 5.5, 7, 15, 20.25, 22, and 46 hours.

segregation-driven dynamic equilibrium resembling the exponential stationary solution of the continuity equation. At the same time, on the carbon surface, there is no evidence of a preferential segregation of the deuterated component, and the diffusion progresses without producing a steady state even after 46 hours.

A finite-element algorithm based on the continuity equation, similar to the one described earlier, was used to fit the SIMS results. A rectangular profile was taken as an initial condition. The computer-generated solutions were compared with the experiment, after each time-step, by means of calculating square average of the difference. Once a best fit was determined for a given experimental depth profile, this fit was then used as the initial condition for the subsequent annealing time. This incremental approach introduced in [2], while slightly increasing the computational error, no longer averages D over the entire annealing time for each fit. In this way the time dependence of D could be deduced from each temporal interval.

The fits, at a given annealing time, employed an assumed power law dependence on depth for the unitless diffusion coefficient, of the form

$$d(x) = a + (x_t - x)^b .$$

This dependence allows a non-zero diffusion coefficient at the interface. Exponents (b) of 0 (no depth dependence), ½, 1, 3/2, and 2 were examined. Broadening of the experimental profiles due to the finite depth resolution of SIMS was accounted for by convolving the computer solutions with a Gaussian before fitting, where the width of the Gaussian was derived from a fit of the unannealed profile.

In the Appendix we provide one of the codes employed to actualize the algorithm described above. It is written in Microsoft QuickBasic and yields an output in ASCII format.

Evidently, the segregation terms have almost no effect on the analysis of the C sample. In this case, the analysis is a straightforward, standard application of Fickian diffusion. Therefore, while fitting the C-surface results, the segregation contribution was excluded from the algorithm.

It was found that for almost all the annealing times involved, the best fit is obtained with the diffusion scaling with depth as the power of 3/2, which is in excellent agreement with the behavior previously observed in [4]. With this assumed power law, only a single fitting parameter (a) is required to obtain the best fit. The best fit yields a plot of the relative diffusion coefficient $d(x)$ as a function of depth x. The absolute value of the diffusion coefficient $D(x,t)$ is proportional to $d(x)$, with its magnitude determined from the known experimental annealing time.

In Figure 3.8, we show several plots comparing experiment with the computer-generated profiles for the carbon surface. SIMS data are overlapped with the best fits obtained using a uniform (0-power law) and a depth-dependent (3/2-power law) model for the diffusion coefficient. It is obvious that a uniform diffusion coefficient provides a poor fit to the experimental results. We accept this as yet another confirmation of diffusion inhibition near the polymer/solid interface.

Fig. 3.9 illustrates the evolution of the diffusion curve with time for the carbon-surface samples. One can see a significant drop in the value of the diffusion coefficient at both carbon and vacuum interfaces over the period of 46 hours. The same trend can be seen in Fig. 3.10, showing the time dependence of solid and

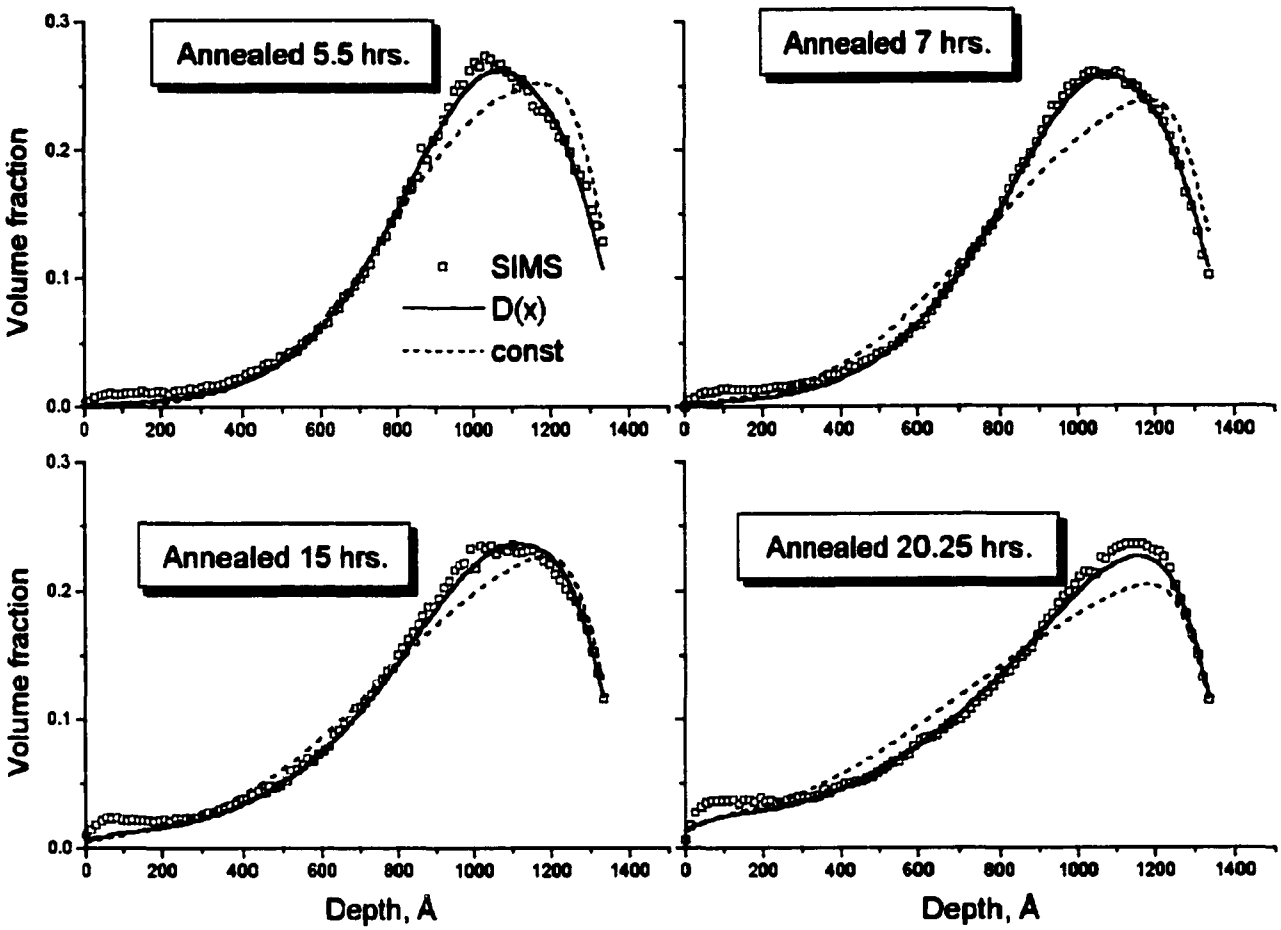

Figure 3.8 The experimental SIMS profiles (squares) for anneals of 5.5, 7, 15, and 20.25 hours on the carbon surface are contrasted to the numerical best fits obtained assuming a 3/2-power scaling with depth for D (solid line) and a constant value of D (dashed line).

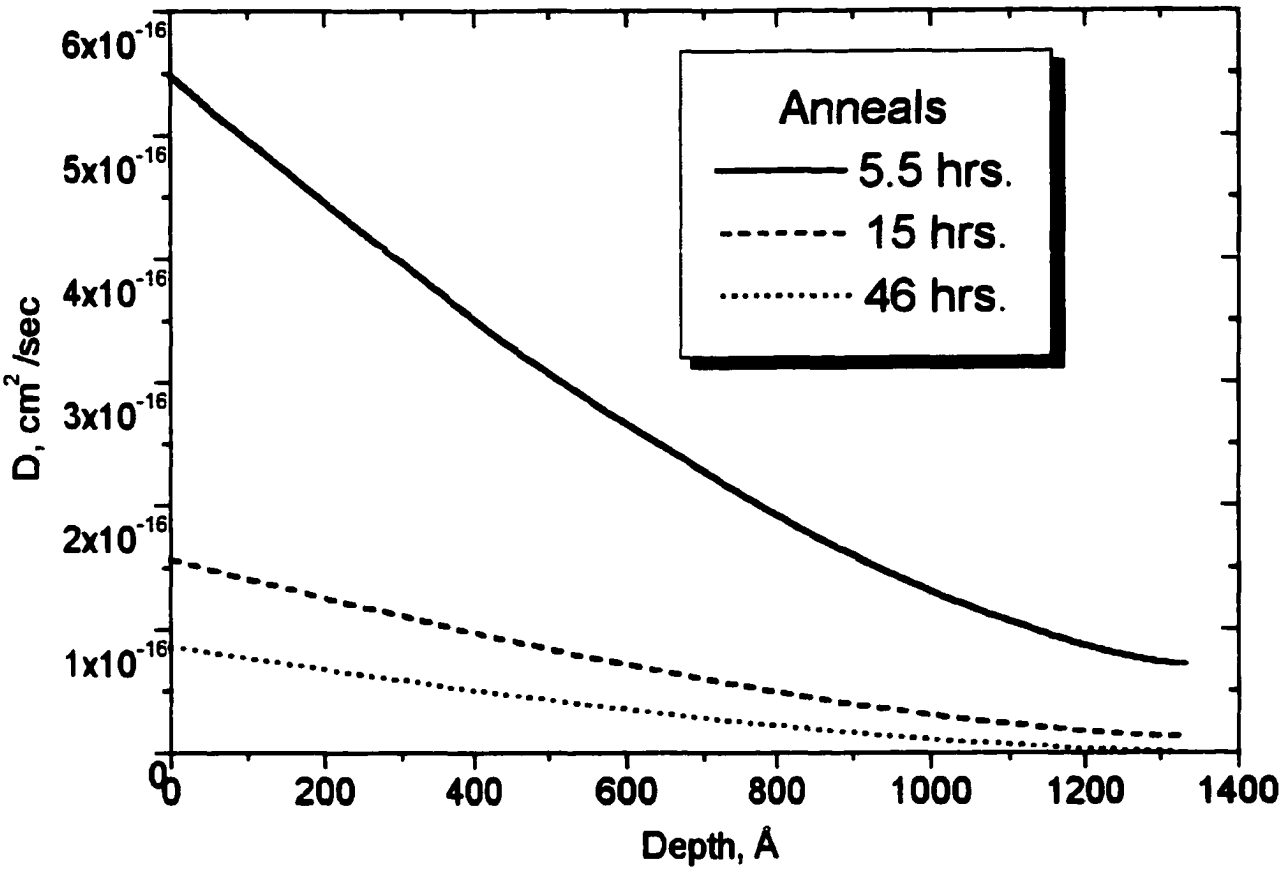

Figure 3.9 Evolution of the depth-dependent diffusion coefficient (with best 3/2 power laws fits) for the samples on the carbon surface annealed for 5.5, 15, and 46 hours.

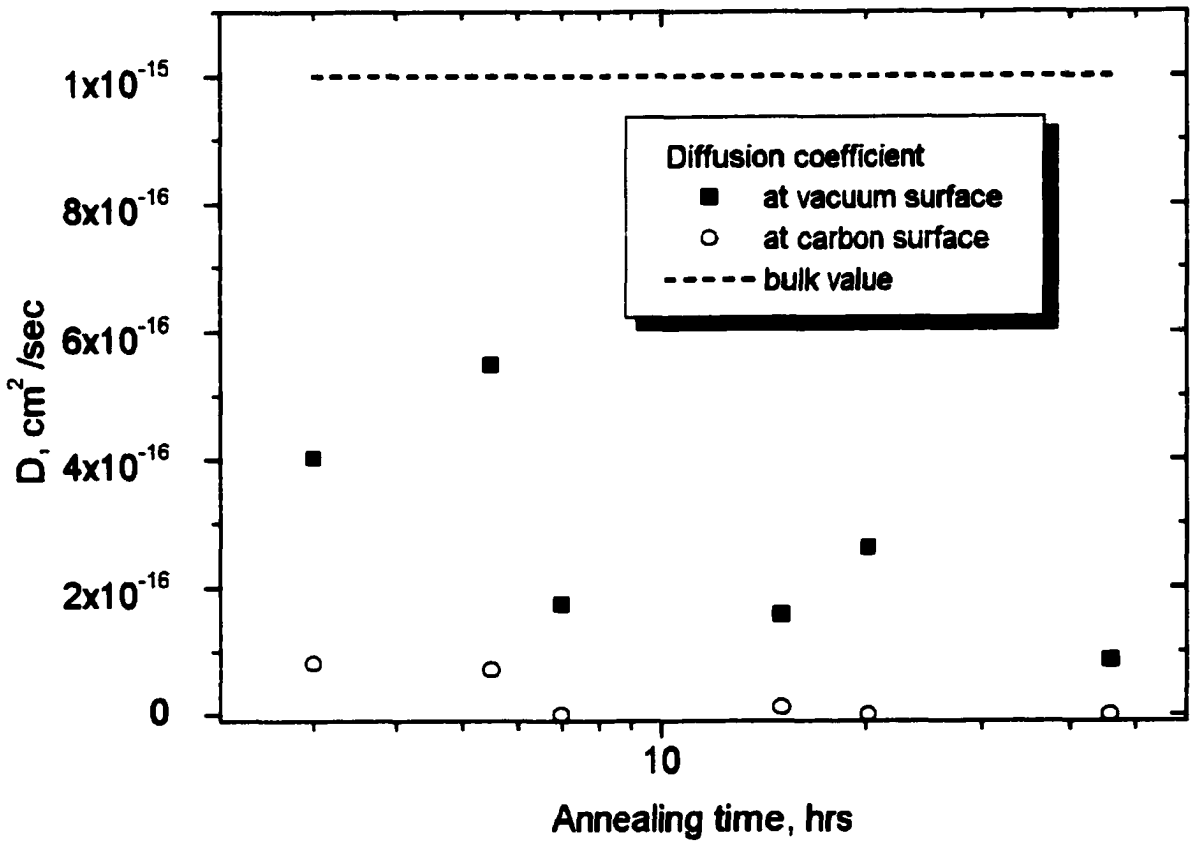

Figure 3.10 Time dependence of the calculated diffusion coefficient near the vacuum (squares) and carbon (circles) interfaces. The dashed line indicates the predicted bulk value [12].

vacuum boundary values of D for the C substrate, and the bulk value predicted in [12]. The data in this figure appears noisy, and it requires further comment. Some noise results from the use of the prior sample fit as an initial starting condition, so that if the annealing times are close together, a larger error is probable. Also, the vacuum surface data plotted are obtained by extrapolating the values of D to the boundary with a very low concentration of material. It might introduce extra uncertainty, especially for shorter annealing times.

For the silicon interface, the fitting procedure is more problematic because of the strong segregation and the fast formation of the equilibrium distribution. But the calculated values of the diffusion coefficient fall within the same range as for the carbon interface. For instance, an extrapolation to the vacuum surface produces an estimate for D of 5.7×10^{-16} cm^2/sec for 3 hours and 2.0×10^{-16} cm^2/sec for 5.5 hours of annealing time.

Finally, in Fig. 3.11 we plot the extrapolated values of function $g(t)$ normalized to the square of the gyration radius as a function of time in units of the reptation time. The result is fit by the power law very close to the $t^{1/2}$-scaling regime. Even after tens of reptation times there is no evidence of transition to the usual linear dependence on t predicted by the reptation theory.

While the results of this study do not conclusively favor a particular model of diffusion modification mechanism, an eventual detailed description of interfacial behavior will certainly have to account for the time dependence of diffusion. This report is among a few addressing the long-scale kinetics issue. The observed nontrivial time behavior may require introduction of a new characteristic time scale. We exclude the possibility of a strong effect of the initial stress relaxation in

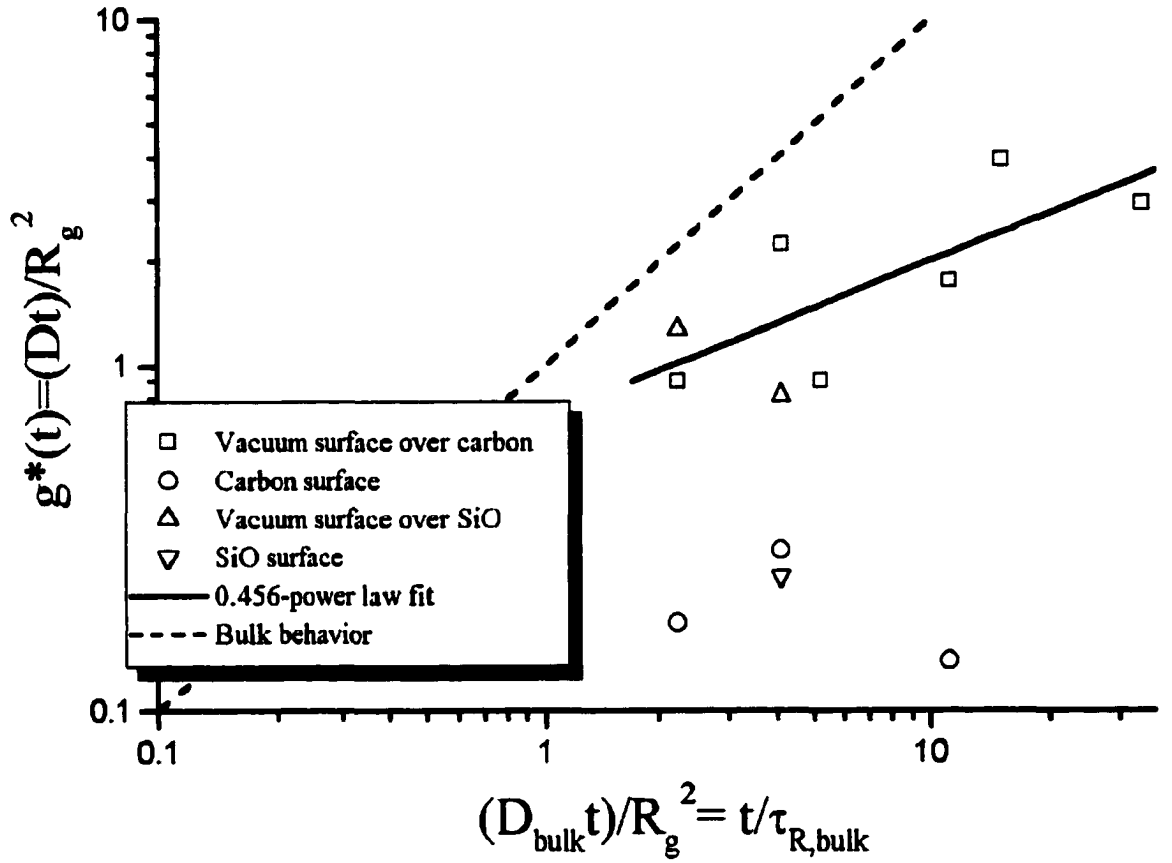

Figure 3.11 Extrapolated values of $g(t)$, normalized to the square of the bulk gyration radius, as a function of time in units of the bulk reptation time. The results at the vacuum surface are fit by a power law of 0.456, very close to the $t^{1/2}$-scaling regime. Even after tens of reptation times there is no evidence of transition to the usual linear dependence on t predicted by the reptation theory.

the spun bottom PS layer. The annealing temperature is much higher than the T_g bulk value and one would expect relatively fast redistribution of a stressed conformation. The fact that even for the longest annealing times the chains have moved only a distance comparable to R_g may render a plausible explanation for the time scaling behavior. Within the assumption that the reptation time is significantly longer at the wall due to the entanglement pile-up, one can speculate that the melt is still in the regime when the reptating chains have not left their initially entangled conformations completely.

We are currently designing a modified procedure for the TOF-SIMS instrument to extend our capabilities and improve the accuracy of results. The *in-situ* annealing feature will allow us to run depth profiles for consecutive anneals on a single sample, possibly containing more than one dPS marker layer. Along with the better depth resolution, this feature will be able to reduce the experimental and computational noise. With the new primary ion source, lateral diffusion studies will elucidate more features of anisotropy and time evolution. Surfaces other than Si and C should be of interest as well.

References:

1. Y. Strzhemechny, V. Shapovalov, K. G. Zhou, S. A. Schwarz, J. Sokolov, and M. H. Rafailovich, in *Proceedings of MRS 98 Fall Meeting*, (Boston, 1999).
2. Y. Strzhemechny, V. Zaitsev, K. Zhou, S. A. Schwarz, J. Sokolov, and M. H. Rafailovich, submitted to *High Performance Polymers*.
3. G. Coulon, T. P. Russell, V. R. Deline, and P. F. Green, *Macromolecules* **22**, p.2581 (1989).

4. S. J. Whitlow and R.P. Wool, *Macromolecules* **22**, p.2648 (1989).

5. X. Zhao, W. Zhao, J. Sokolov, M. H. Rafailovich, S. A. Schwarz, B. J. Wilkens, R. A. L. Jones, and E. J. Kramer, *Macromolecules* **24**, p.5991 (1991).

6. X. Zheng, B.B. Sauer, J.G. Van Alsten, S.A. Schwarz, M.H. Rafailovich, J. Sokolov, and M. Rubinstein, *Phys. Rev. Lett.* **74**, p.407 (1995).

7. X. Zheng, M. H. Rafailovich, J. Sokolov, Y. Strzhemechny, S. A. Schwarz, B. B. Sauer, and M. Rubinstein, *Phys. Rev. Lett.* **79**, p.241 (1997).

8. X. Zhao, Ph.D. thesis, CUNY (1993).

9. H. Nakanishi and P. Pincus, *J. Chem. Phys.* **79**, p.997 (1983).

10. I. Schmidt and K. Binder, *J. Phys. (Paris)* **46**, p.1631 (1985).

11. R. A. L. Jones, E. J. Kramer, M. H. Rafailovich, J. Sokolov, and S. A. Schwarz, *Phys. Rev. Lett.* **62**, p.280 (1989).

12. P. F. Green and E. J. Kramer, *Macromolecules* **19**, p.1108 (1986).

13. R. J. Composto, J. W. Mayer, E. J. Kramer, and D. M. White, *Phys. Rev. Lett.* **57**, p.1312 (1986).

14. Y. Zhang, S. Ge, B. Tang, M. Rafailovich, J. Sokolov, D. G. Peiffer, J. A. Dias, K. O. McElrath, S. Schwarz, and S. Satija, BAPS **44**, No.1, Pt I, p.613, paper KP01 170 (1999).

CHAPTER 4

Secondary ion mass spectrometry study of silicon surface preparation and the polystyrene/silicon interface

Silicon wafer surfaces are frequently subjected to a wet chemical cleaning process prior to device fabrication or growth of an epitaxial layer (See [1] for details). In our studies of thin polymer films, especially by SIMS, we often employ chemically cleaned silicon wafers as supporting substrates. The chemical state of the silicon surface, which may for example be oxidized or hydrogen terminated, can affect the behavior of mobile components near the polymer/silicon interface, as a result of a change in the free energy or reactivity of the silicon surface. One such study [2] is described in Chapter 3, where the diffusion coefficient of PS has been compared at a native SiO surface, a thin PVP film surface, a vacuum surface, and a hydrogen passivated Si surface obtained as a result of chemical processing. Also, in contrast to the hydrogen terminated Si surface, enhanced segregation [3] or grafting [4] have been observed at oxidized silicon surfaces.

The advantage of an ultraclean atomically smooth substrate for these high-resolution studies is clear, although certain concerns exist. There is a possibility that a remnant layer of moisture exists at the polymer/silicon interface as the result of the chemical processing involving wet etching or due to a subsequent atmospheric exposure. Moisture could impact the chemistry of the interfacial region during sample annealing. It is important therefore to determine the effect of

wet chemical cleaning procedures on the polymer/silicon interface.

In this chapter, based on our report [5], we investigate the conditions of the silicon surface subject to a wet etching procedure. SIMS is employed to obtain depth profiles of deuterium, oxygen, and other constituents at the polystyrene/silicon interface. Deuterated etching solutions are utilized, so that the observed deuterium profiles may be associated with a particular etching/cleaning step. The effect of annealing on the interface is examined, to determine if interfacial contaminants are mobile. Results are compared with spectroscopic studies of the bare silicon surface, as well as with studies of diffusion and segregation near the polymer/silicon interface.

A modified Shiraki etch [6] is employed in this study. For this commonly employed technique, the silicon surface is immersed in an 80°C 4:1:1 $H_2O/H_2O_2/NH_4OH$ bath for 5 minutes, and then rendered hydrophobic by a 30 second room temperature exposure to 30% concentration HF. Following this step, and a brief 30 second rinse in deionized water, the sample is immersed in an 80°C bath of 5:1:1 $H_2O/H_2O_2/HCl$ for 5 minutes, resulting in the formation of a thin oxide layer. A 30 second water rinse is again performed, and the thin oxide layer is then removed in a second HF etch. This etching cycle may be repeated two or three times. The state of the silicon surface following the HF etch has been examined by numerous workers. Recent studies, for example, by infrared spectroscopy [1], x-ray photoelectron spectroscopy [7], [8] and thermal desorption spectroscopy [9] confirm that the HF treated silicon surface is terminated by a monolayer coverage of hydrogen. This hydrogen passivated silicon surface has excellent chemical stability. If immersed in water, the topmost layer of silicon is oxidized only after

several minutes, while the second layer is oxidized after a period of weeks [8].

PS films of molecular weight 65K and of thickness 1100 Å were spin-coated onto (100) silicon wafers. The silicon samples were either in the as-received condition (covered with ca. 15 Å of native oxide), or had received the modified Shiraki cleaning procedure described above. A variety of cleaning procedures were employed, in which a 30% solution of HF in D_2O was substituted for the normal solution, and samples were examined just after the HF etch and water rinse, or following the subsequent peroxide/HCl (either normal or deuterated) oxidizing step. The water rinse was assumed to have little effect on the chemically stable hydrophobic surface. The deuterated HF solution was employed shortly after mixing D_2O with HF, but as a check, in several samples the HF solution was allowed to equilibrate for approximately two hours. No significant difference in the extent of deuterium coverage at the interface was observed by SIMS in these two cases. Each sample was cleaved into two pieces, and one piece was annealed at 190°C in a vacuum of about 10^{-2} Torr for periods of 15 minutes to 2 hours.

It should be noted that the observed diffusion coefficient of PS on the silicon oxide or stripped surfaces is approximately 4×10^{-16} cm^2/s at 167°C for a molecular weight of 65K. For the annealing conditions employed in the present study, diffusion at this rate would be easily observable. Also, blends of dPS and PS were annealed in vacuum at 184°C, a temperature that ensures that the blend is in a bulk single-phase regime [10]. The deuterated component segregated to the silicon surface and to the vacuum interface, and was falling off in concentration with a decay length of approximately 200 Å, well resolved by the SIMS technique. The SIMS technique should therefore be sensitive to the motion of deuterium

incorporated into the polystyrene from a contaminated silicon surface as a result of either diffusion or segregation.

The SIMS conditions employed were as described in the previous chapters. Negative secondary ions were monitored, allowing the ready detection of O, Br, F, Cl, and S ions, which are preferentially emitted as negative ions, and permitting detection of D without concern for an H_2 interference. Samples were positioned to avoid spurious contributions from particulates or inclusions, which become apparent in the imaged surface distributions of O^- or F^- that are monitored during the SIMS depth profile. The implantation standards for D, O, and F in Si were examined under 12 keV argon bombardment (affording high sensitivity but poor depth resolution as compared to 2 keV bombardment), in order to obtain a rough quantitative measure of the observed interfacial concentrations. It is reasonable to assume that the ratios of the D, O, or F signals to the Si signal within the silicon are only weakly dependent on the argon bombardment energy. Depth scales were calibrated by measuring sputtered crater depths with a stylus profilometer, while depth scales in the polymer films were determined from the known film thicknesses as determined by ellipsometry. Aside from the implantation standards, all other samples were examined under 2 keV argon bombardment. A thick thermal oxide on silicon was profiled as an alternate standard for oxygen. A blend of 20% dPS/80% PS (molecular weights of 550K and 670K, respectively) with a deposited thickness of 300, 1000, or 3000 Å, was spin-coated onto as-received (native oxide) samples, and onto hydrogen terminated surfaces prepared as above. The samples were annealed in a vacuum of 10^{-2} Torr at 165°C for five days. An additional 400 Å PS layer was then floated onto each sample as a

protective sacrificial layer. These samples allow quantitation of the D^- and CD^- signals within the polystyrene. The depth profiles obtained in these two samples are illustrated in Fig. 4.1. Segregation of the deuterated component is apparent at the vacuum interfaces, and enhanced segregation is apparent at the native oxide interface. The D^- and CD^- profiles (not shown) mirror each other closely. The F^- and O^- signals show contamination at the PS silicon interface and at the float interface, but these species undergo minimal diffusion during the anneal.

Figure 4.2 shows intensities of the D^-, CD^-,O^-, and F^- secondary ion intensities, in arbitrary units, as a function of depth for the 1100 Å undeuterated PS film. The illustrated sample received a final D_2O/HF etch and was not annealed. The interfacial deuterium peak has a full width half-maximum (FWHM) of 120 Å, which is consistent with the known resolution of the technique for the conditions employed, though slightly larger than the widths of the O of F peaks described below. Assuming that the sensitivity factor required to convert the D^- signal (after normalizing to the bulk silicon signal level) to true concentration is the same as the sensitivity factor derived from the implantation standard, the total integrated dose of D in the interfacial peak is calculated to be 6×10^{15} cm^{-2}, which is on the order of one monolayer of coverage as expected. If the sensitivity factor used for the conversion is derived from the blend of Fig. 4.1, the integrated dose is approximately a factor of 5 lower. Evidence cited below suggests that the D is not associated with the polymer, although the true sensitivity factor at the interface is uncertain by at least a factor of 2. The CD^- signal shows a relatively high background within the PS layer (perhaps due to CH_2^-), corresponding to an apparent deuterated fraction of about 1 %. In deuterated blends, the D^- and CD^-

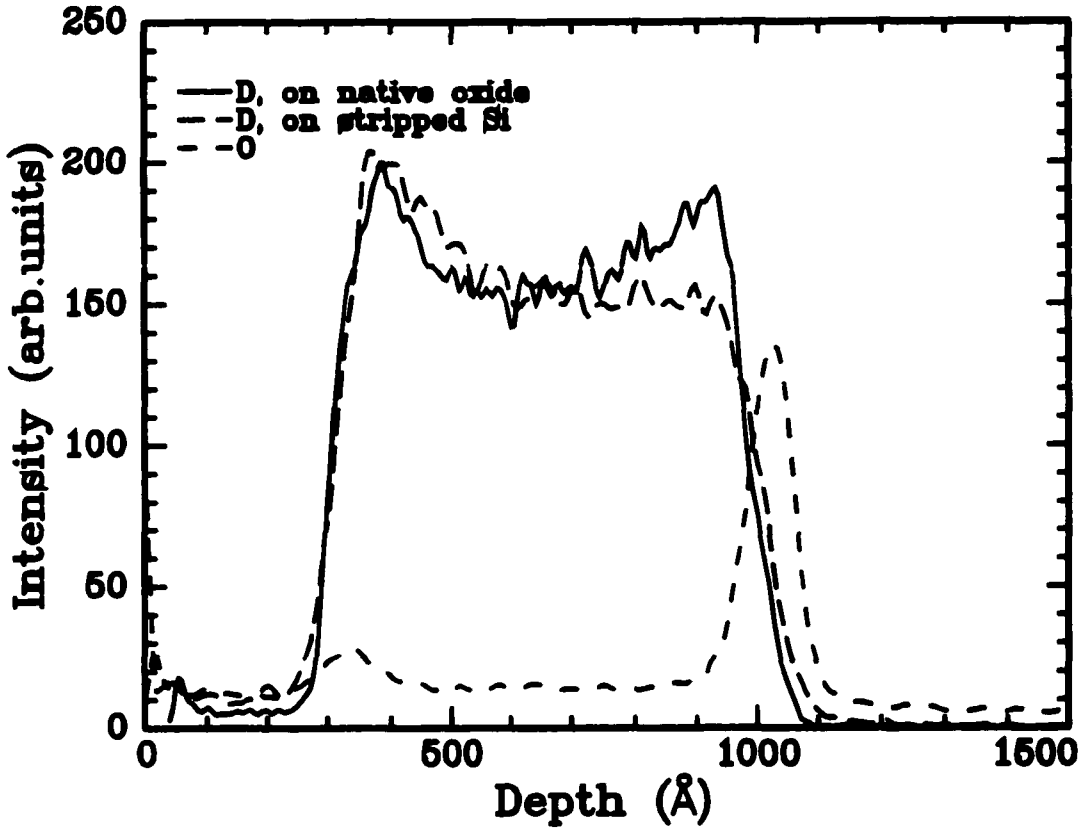

Figure 4.1 D^- depth profiles of 20% dPS/80% PS blends spin-coated onto native oxide and HF stripped silicon. The illustrated O^- profile is from the stripped sample. Strong deuterium segregation is observed at the native oxide surface.

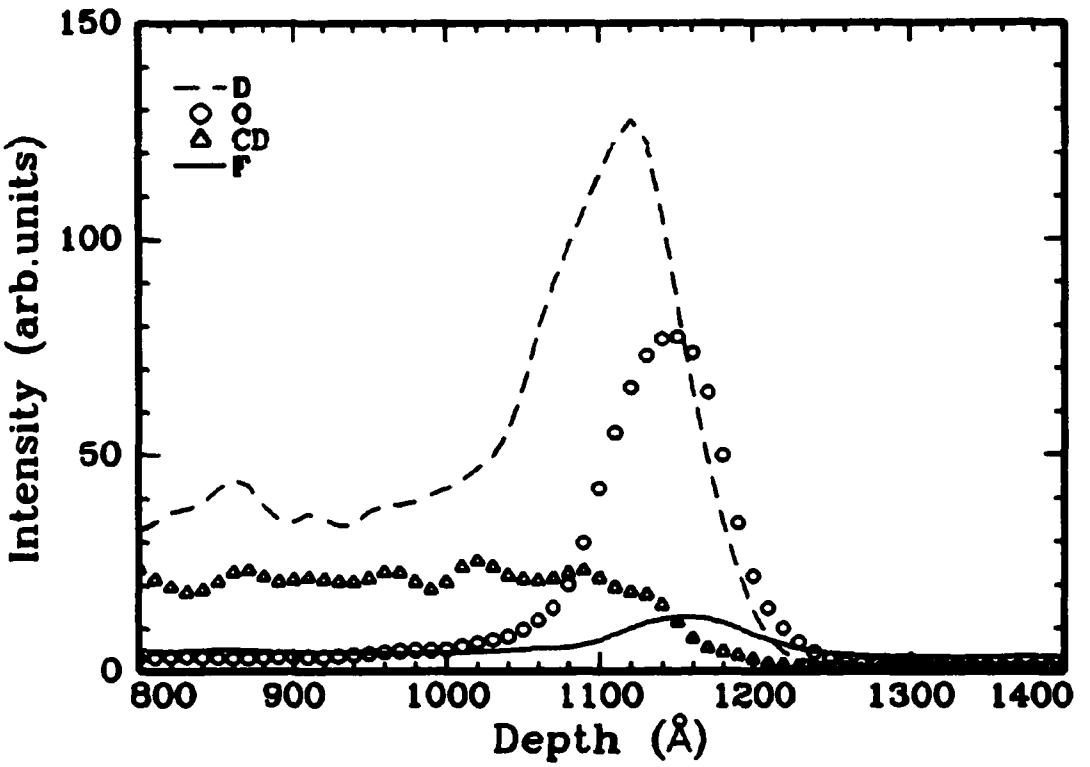

Figure 4.2 SIMS depth profile of the unannealed PS/silicon interfacial region for an HF stripped surface. The peak widths are resolution limited. The absence of a CD^- peak indicates that deuterium is associated with the silicon surface and not with neighboring PS chains. Quantification of the illustrated concentration levels by the use of standard samples is described in the text.

intensities are comparable, so that if the D is associated with polymer chains at the interface, an interfacial peak of CD should be in evidence. Such a peak is not observed in any of the profiled samples.

The amount of oxygen at the interface is difficult to quantify. If the sensitivity factor derived from the dilute oxygen implant standard is employed, the apparent concentration of oxygen at the interface exceeds the maximum possible value. If, on the other hand, the sensitivity factor derived from the thick thermal oxide standard is employed, the apparent peak oxygen concentration in the interfacial region does not exceed 1 atomic %. This implies that the oxide sensitivity factor can not be used since this region does not have sufficient oxygen to resemble a thermal oxide. The large difference in sensitivity factors results from the high ionization probability of oxygen ions emitted from silicon dioxide. The width of the peak is again resolution limited, and it is clear that the areal density of oxygen at the interface must be a small fraction of a monolayer.

The fluorine concentration appears to peak slightly within the silicon layer. This finding is consistent with recent XPS studies of hydrogen-terminated Si wafers [11] showing evidence of subsurface F atoms. Sputtered fluorine atoms have a high probability of emerging from the sample surface as negative ions, yielding high sensitivity. The concentration within the silicon is dilute, and it appears reasonable to apply the sensitivity factor derived from the implant standard. In this case, the total dose of fluorine contained in the interfacial region is $6x10^{12}$ cm^{-2}. Comparable fluorine peaks are observed in all samples and are relatively unaffected by annealing or by the energy or flux of the argon ion beam. Graf, *et al.*[7] notes that the surface F concentration decreases rapidly with time

spent in the deionized water rinse, dropping to the lowest detectable levels by x-ray photoelectron spectroscopy (XPS), in the low 10^{13} cm^{-2} range, after about one minute of immersion.

Figure 4.3 contrasts two unannealed samples. One sample is coated with PS shortly after the deuterated HF etch. The second sample receives an HF etch step followed by a deuterated peroxide/HCl exposure. As expected, the interfacial deuterium peak is largely removed, and significantly more interfacial oxygen is present in the second sample. The width (FWHM) of the oxygen peak is 90 Å and is unaffected by the increased oxygen concentration. The deuterium peak present after a deuterated HF etch step was reduced dramatically in all of the samples examined following either a deuterated or normal peroxide/HCl exposure.

Figure 4.4 compares an unannealed and an annealed sample (190°C, 15 min). The sample again has received a deuterated HF etch immediately prior to spinning on a PS layer. The anneal has no appreciable effect on the D^- or O^- interfacial peaks. An upper limit on the diffusion coefficient for D may be derived from these profiles of 2×10^{-16} cm^2/s, which is more than four orders of magnitude smaller than the bulk diffusion coefficient of 65K PS at 190°C. There is no evidence of the presence of deuterium within the polymer layer, as evidenced especially by the lack of a CD peak in any of the samples, following treatment in deuterated HF or deuterated peroxide/HCl solution. It is reasonable to conclude that any moisture present as the result of the cleaning process cannot exceed a level of a fraction of a monolayer, and does not appear to pose a limitation for polymer/silicon interfacial studies.

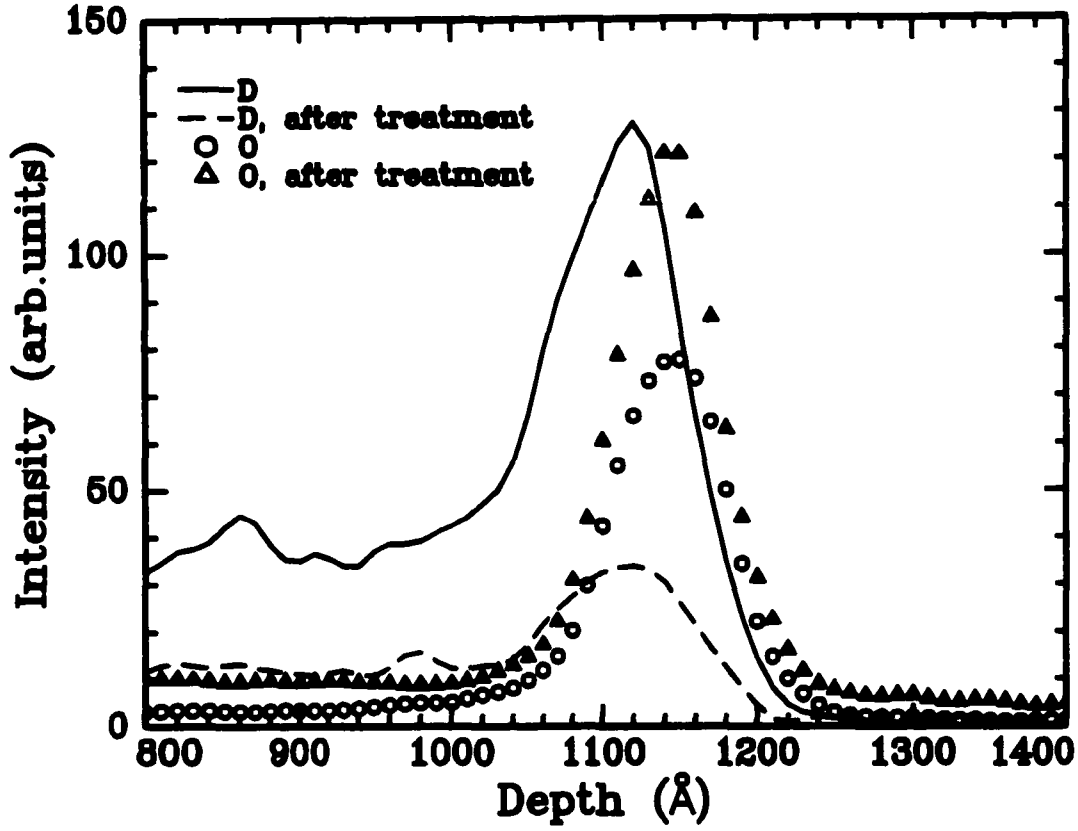

Figure 4.3 Comparison of D^- and O^- peaks at an HF stripped surface before and after exposure to a deuterated peroxide/HCl solution. The deuterium level is much reduced, and the oxygen concentration increases, although the peak width is unaffected.

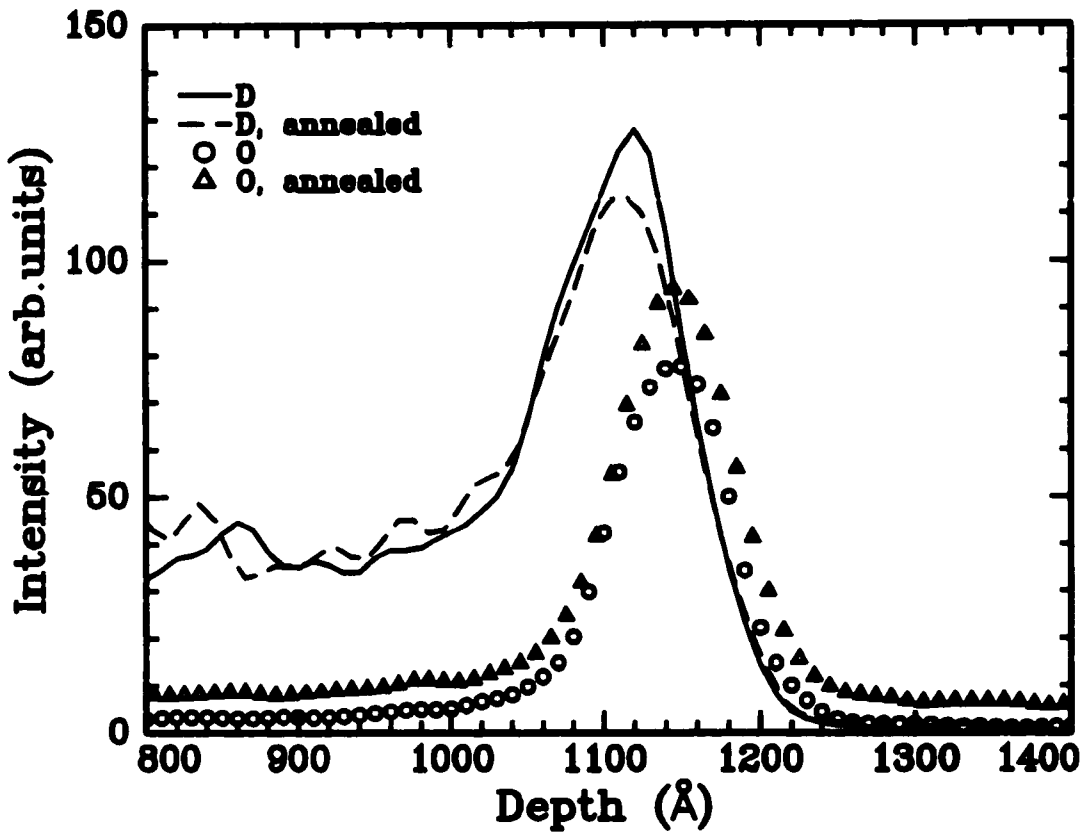

Figure 4.4 D^- and O^- SIMS depth profiles in an unannealed and an annealed (190°C, 15 min) PS film on HF stripped silicon. The anneal has no appreciable effect on the D^- or O^- interfacial peaks.

References:

1. G. W. Trucks, K. Raghavachari, G. S. Higashi, and Y. J. Chabal, *Phys. Rev. Lett.* **65**, p.504 (1990).
2. X. Zheng, B.B. Sauer, J.G. Van Alsten, S.A. Schwarz, M.H. Rafailovich, J. Sokolov, and M. Rubinstein, *Phys. Rev. Lett.* **74**, p.407 (1995).
3. S. A. Schwarz, B. J. Wilkens, M. A. A. Pudensi, M. H. Rafailovich, J. Sokolov, X. Zhao, W. Zhao, X. Zheng, T. P. Russell, and R. A. J. Jones, *Mol. Phys.* **76,** p.937 (1992).
4. Y. Liu, S. A. Schwarz, W. Zhao, J. Quinn, J. Sokolov, M. Rafailovich, D. Iyengar, E. J. Kramer, W. Dozier, L. J. Fetters, and R. Dickman, *Europhys. Lett.* **32**, p.211 (1995).
5. Y. M. Strzhemechny, S. A. Schwarz, J. Schachter, M. H. Rafailovich, and J. Sokolov, *J. Vac. Sci. Technol. A* **15**, p.894 (1997).
6. J. Phillips, L. Pfeiffer, D. C. Joy, P. P. Smith III, J. M. Gibson, W. M. Augustyniak, and K. W. West, *J. Electrochem. Soc.* **133**, p.224 (1986).
7. D. Graf, M. Grundner, and R. Schulz, *J. Vac. Sci. Technol. A* 7, p.808 (1989).
8. U. Neuwald, *J. Appl. Phys.* **78**, p.4131 (1995).
9. K. Kinoshita and I. Nishiyama, *J. Vac. Sci. Technol.* A **13**, p.2709 (1995).
10. R. A. L. Jones, E. J. Kramer, M. H. Rafailovich, J. Sokolov, and S. A. Schwarz, *Phys. Rev. Lett.* **62,** p.280 (1989).
11. Y. Morikawa, K.Kubota, H. Ogawa, T. Ichiki, A. Tachibana, S. Fujimura, and Y. Horiike, *J. Vac. Sci. Technol. A* **16**, p.345 (1998).

CHAPTER 5

Other results for polymer properties probed with surface sensitive techniques

During his stay in the Doctoral Program of CUNY, the author of this thesis participated in a variety of related research projects, reported in [1]-[10]. The results were obtained in cooperation with other participants of the Garcia Center. In this chapter, I will briefly outline the most interesting of those results accomplished with a direct contribution of the author.

Modification of polymer properties due to interfacial phenomena is not limited to the case of a solid wall only. Interesting and unusual effects may occur at the polymer/polymer boundary as well. In [3], SIMS depth profiling was employed to monitor the interfacial behavior between two ionomer films. Ionomers are copolymers having functional groups capable of forming strong ionic interactions. Because of the presence of such groups, an additional characteristic time comes into play, namely a lifetime of an ion pair in a multiplet. Depending on the degree of polymerization between ionic pairs on the chain, the dynamic properties of ionomers may exhibit a significant diversity. It is possible to attain a regime for which the exchange hopping of the ions between the multiplets occurs much faster than the motion of the backbones (the so called 'fast exchange'). Such behavior was observed in the cited study. A bilayer of two ionomer films was prepared. The ionomers used were lightly sulfonated polystyrenes, neutralized with Na or Rb

(PSS-Na or PSS-Rb), and their deuterated counterparts (dPSS-Na or dPSS-Rb). A top 600 Å layer of dPSS-Na was floated on top of a 1200 Å thick bottom layer of PSS-Rb deposited on a native oxide of silicon. The samples were annealed at 135°C for 10 min and profiled with SIMS to monitor D^-, Na^+, and Rb^+ concentrations. The obtained profiles, prior and upon annealing, are shown in Fig. 5.1. No center of mass diffusion of the polymer chains has occurred during the annealing. At the same time a substantial amount of ion diffusion has occurred. The diffusion coefficients of the counterions are approximately 3 orders of magnitude larger than those of the polymer chains. This behavior strongly suggests the fast exchange regime.

Aside from the solid interface case, surface segregation from a blend can also be observed at the interface with another polymer immiscible with the blend species. In [2], for layered films of polycarbonate (PC) and styrene-co-acrylonitrile (SAN) blends, SIMS was used to investigate the interfacial adhesion. It was found that in a mixture of SAN chains with different content of acrylonitrile (AN), the component having lower AN content migrates towards the interface. A characteristic SIMS depth profile (Fig. 5.2) shows an interface between PC and SAN mixture before and after annealing (at 160°C for 24 hours). The species monitored is the CN^- dimer, the yield of which is directly proportional to the abundance of AN in SAN. The characteristic double-step feature on the annealed interface affirms a strong tendency of the lower AN component to surface-separate and wet the PC interface. As a result, the adhesion at the interface is enhanced, and it can be controlled, while maintaining desirable bulk mechanical properties.

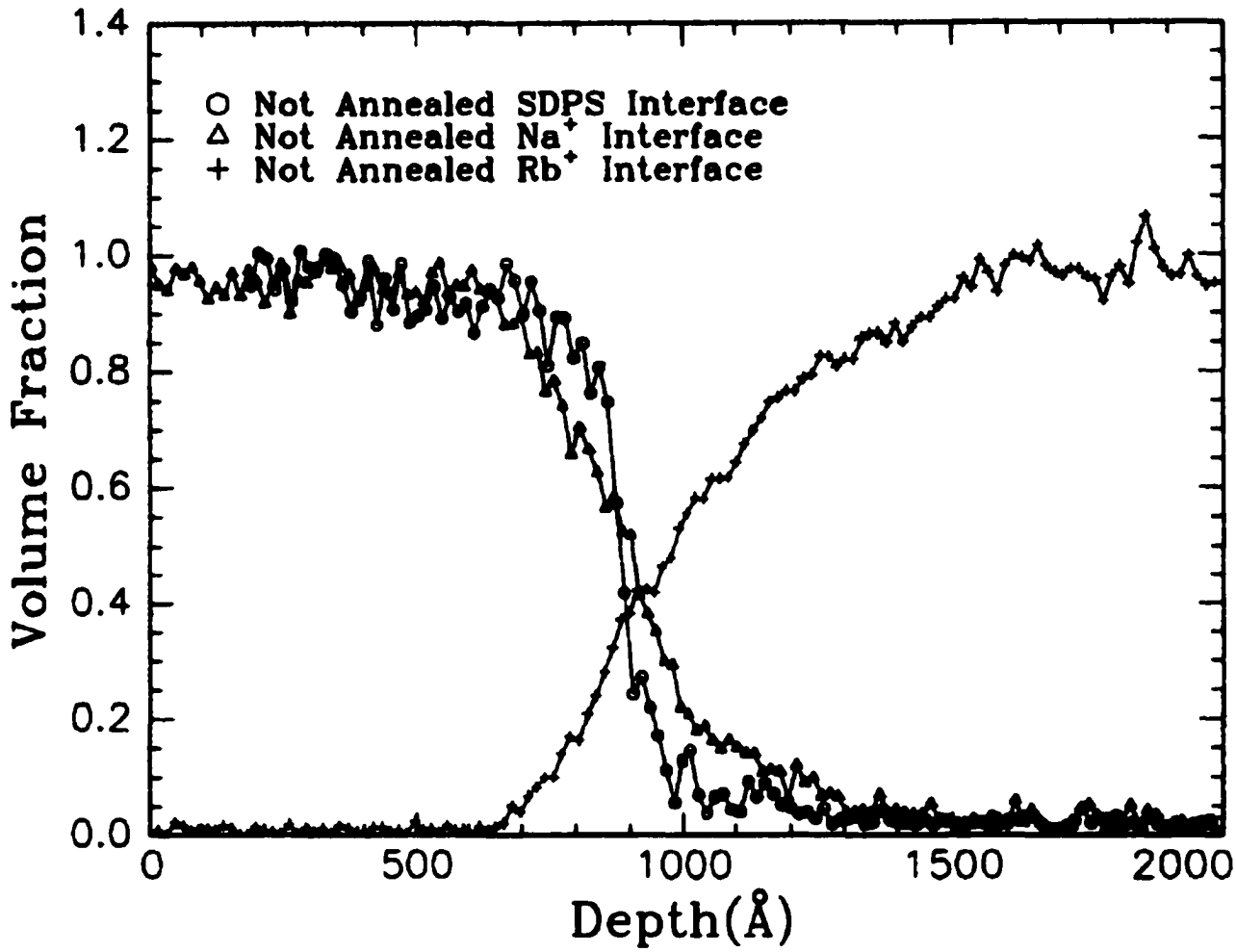

Figure 5.1.a SIMS profiles of deuterium (open circles), Na (open triangles) and Rb (crosses) for dPSS-Na/PSS-Rb before annealing [3].

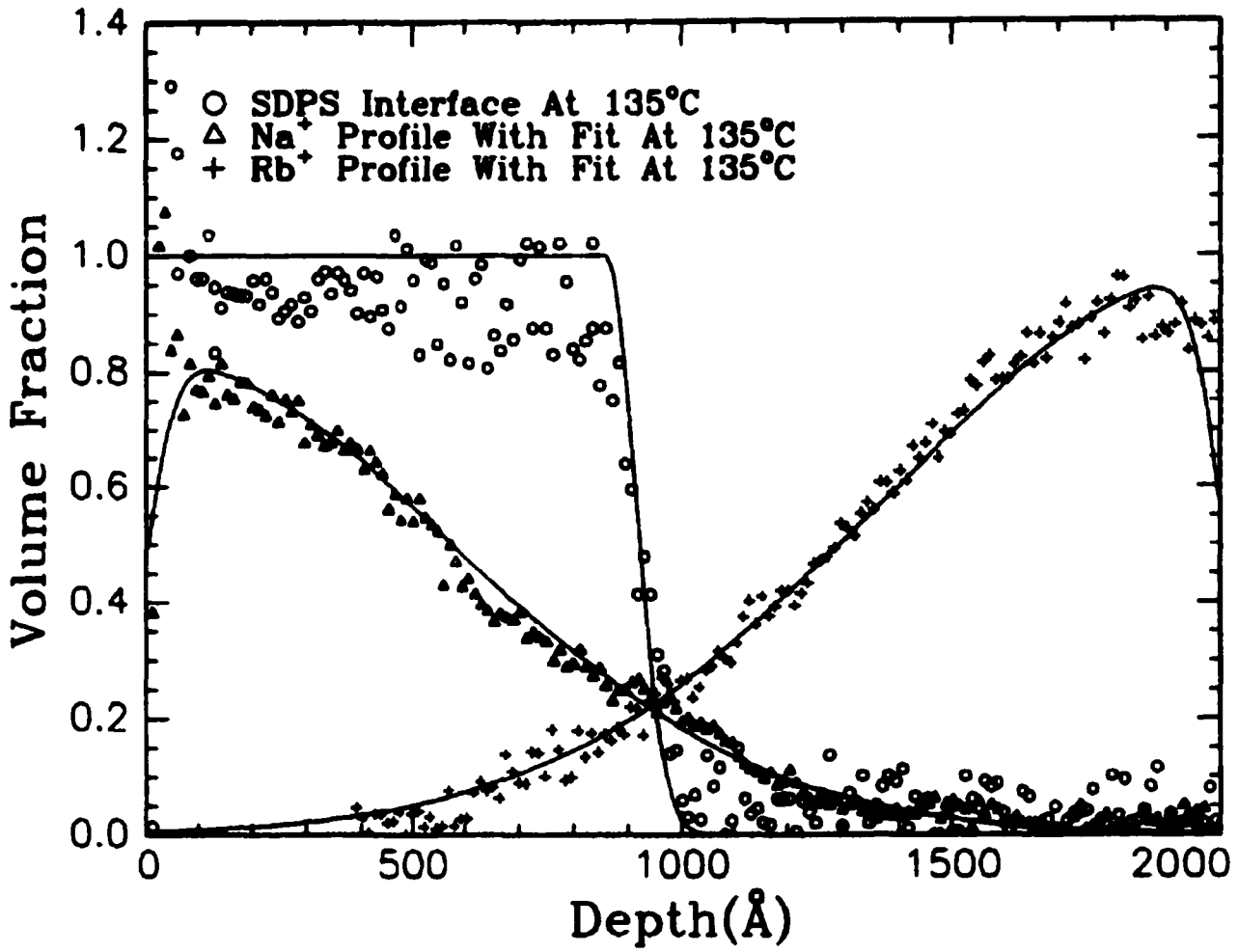

Figure 5.1.b SIMS profiles of deuterium (open circles), Na (open triangles) and Rb (crosses) for dPSS-Na/PSS-Rb after annealing for 10 min at 135°C. Solid curves are the Fickian fits for the counterions and the dPSSNa polymer [3].

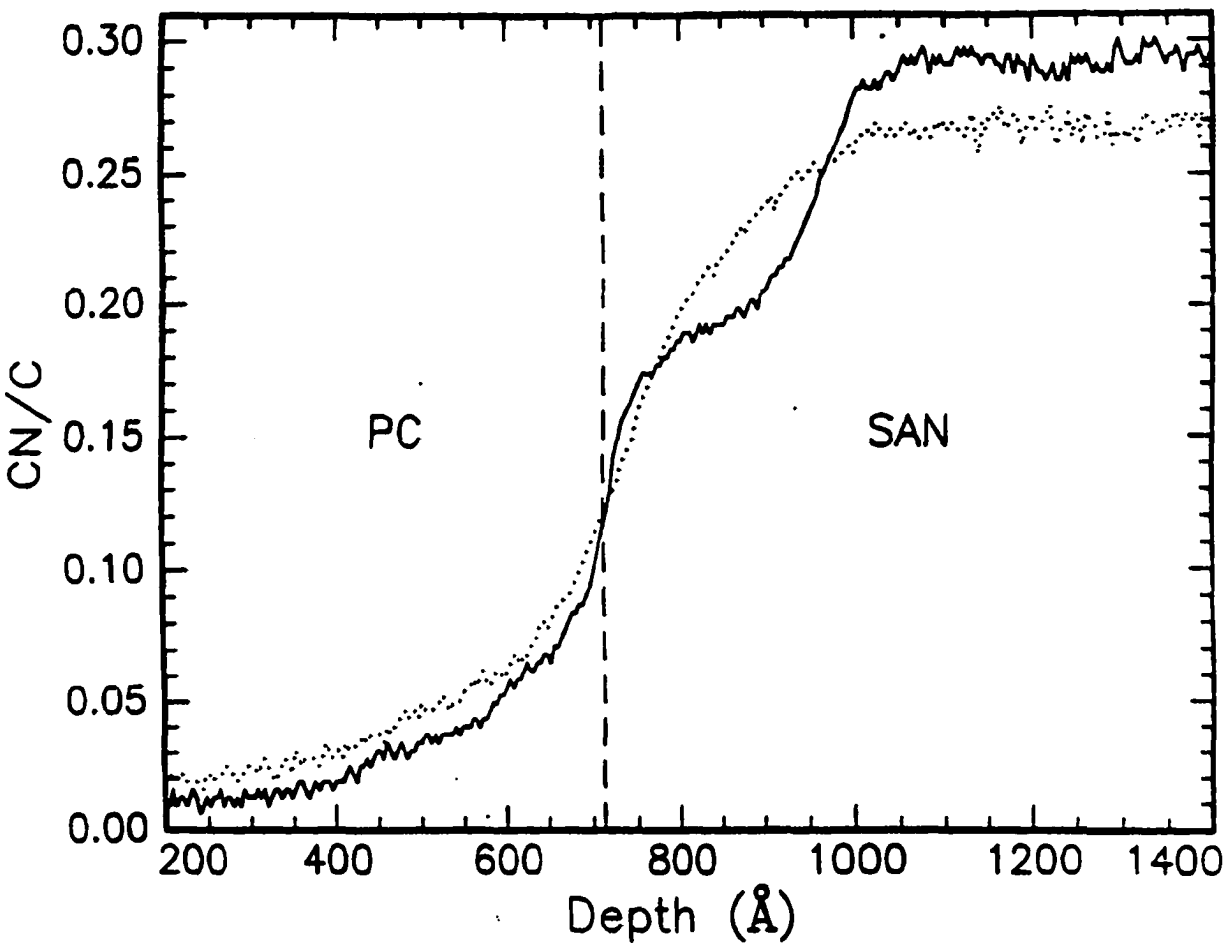

Figure 5.2 SIMS profile of the AN content in a bilayer sample of PC/17%-31% SAN blend. The dotted line corresponds to the unannealed bilayer sample, the solid line corresponds to the sample annealed at 160°C for 24 h. The vertical line marks the original interface [2].

An example of an immiscible polymer blend system was studied in [4], where thin polymer films consisting of a mixture of polystyrene (molecular weight 96K) and poly(*p*-bromo)styrene (PBrS) were also subject to SIMS depth profiling. The films were annealed at 180°C in vacuum and then quenched in air to atmospheric pressure. For a wide range of concentrations, PBrS was found to be encapsulated by PS upon annealing. Figure 5.3 illustrates the encapsulation distribution in the mixture with PBrS volume fraction of 0.4. It is clear that the PBrS concentration drops off at the vacuum and the silicon interface. Additional measurements (atomic force microscopy and scanning transmission X-ray microscopy) combined with the SIMS measurements allowed reconstruction of the three-dimensional encapsulation distribution. The dispersive contribution of the PBrS surface energy could then be estimated.

In [1], SIMS profiling was used to estimate the Flory-Huggins parameter (see Chapter 2) of another immiscible system. The polymers used were diblock PS-PVP blends with the blocks completely immiscible with each other. Usually such blends order themselves into spatially non-uniform and sometimes anisotropic structures such as lamellae, cylindrical and spherical micelles (see Chapter 2). The samples in the cited work were annealed at 165°C and 180°C. A multilayered cylindrical and lamellar structure was shown to exist. Upon formation of the micelle patterns, micelle spacings in microphase-separated films were measured by SIMS, which allowed calculating the enthalpy (Flory-Huggins interaction parameter) for this blend.

X-ray Photoelectron Spectroscopy (see Chapter 1) was also effectively

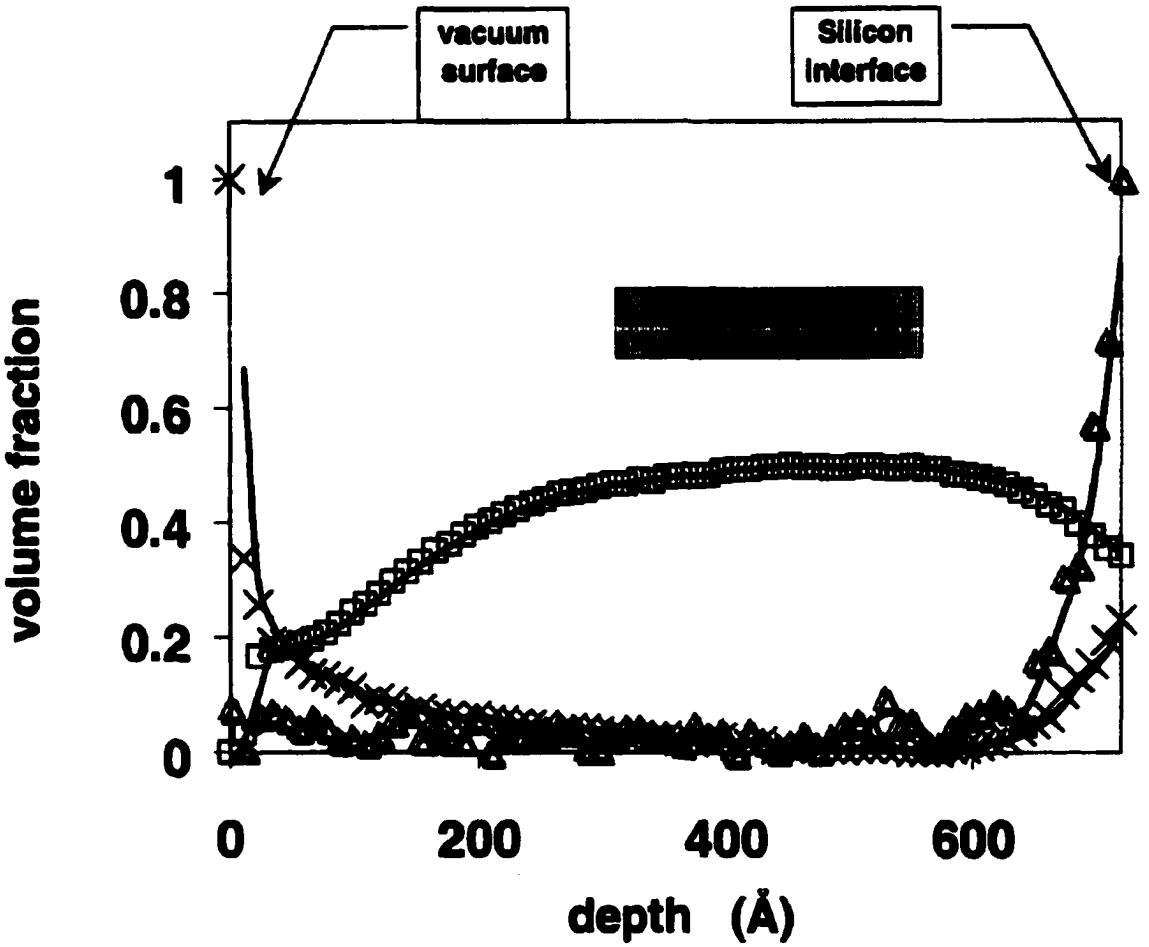

Figure 5.3 SIMS profile of a PBrS/PS blend. The normalized concentration profiles of Br is indicated with open squares. The concentrations of Si (open triangles) and O (crosses) plotted to mark the vacuum and Si interfaces [4].

employed as a tool to probe the surface properties of polymers. In [6] and [7] XPS technique was applied to surface-brominated low-density polyethylene (PE) pellets. In [6] two distinct states of bromine were discovered, suggesting two different types of bromine attachment: in a surface, lamellar-like structure, and a subsurface substitution. In [7], the bromination procedure was augmented by substitution reactions with aromatic thiolate groups. XPS spectra obtained for the samples treated with different substitution groups revealed a significant difference in their sulfur composition. Two distinct sulfur 2p peaks were found to correspond to two different oxidation states of the grafted sulfur. Depending on the aromatic thiolate groups employed in the substitution reaction, the ratio of the two peaks was found to vary dramatically.

Modification of the polyethylene surface is often desirable to alter its poor adhesion properties. The procedure used in [6] and [7] (vapor phase treatment with a subsequent UV exposure) proved to be effective and practical.

References:

1. C. J. Clarke, A. Eisenberg, J. La Scala, M. H. Rafailovich, J. Sokolov, Z. Li, S. Qu, D. Nguyen, S. A. Schwarz, Y. Strzhemechny, and B. B. Sauer, *Macromolecules*, **30**, 4184 (1997).
2. M. Schaffer, V. Janarthanan, Y. Deng, J. La Scala, L. Guo, M. Rafailovich, J. Sokolov, R. S. Stein, Y. Strzhemechny, and S. A. Schwarz, *Macromolecules* **30**, 1225 (1997).
3. R. H. Colby, X. Zheng, M. Rafailovich, J. Sokolov, S. A. Schwarz, Y. Strzhemechny, and D. Nguyen, *Phys. Rev. Letters* **81**, 3876, (1998).

4. D. Slep, J. Asselta, M. H. Rafailovich, J. Sokolov, D. A. Winesett, A. P. Smith, H. Ade, Y. Strzhemechny, S. A. Schwarz, and B. B. Sauer, *Langmuir*, **14**, 4860, (1998).

5. Y. Strzhemechny, S. A. Schwarz, L. T. Guo, X. Zheng, Y. Liu, J. Sokolov, and M. H. Rafailovich, and D. G. Peiffer in *Secondary Ion Mass Spectrometry. SIMS XI*, ed. G. Gillen, R. Lareau, J. Bennett, and F. Stevie (John Wiley & Sons, New York, 1998), p. 481.

6. N. Chanunpanich, A. Ulman, Y. M. Strzhemechny, S. A. Schwarz, A. Janke, H. G. Braun, and T. Kratzmuller, *Langmiur* **15**, 2089, (1999).

7. N. Chanunpanich, A. Ulman, A. Malagon, Y. M. Strzhemechny, S. A. Schwarz, A. Janke, T. Kratzmueller, and H. G. Braun, *Langmuir* **16**, 3557, (2000).

8. Y. Luo, L. Zeng, W. Lin, B. Yang, M.C. Tamargo, Y.M. Strzhemechny, and S. A. Schwarz, submitted to *Semicond. Sci. Technol.*

9. V. Shapovalov, V. Zaitsev, Y. Strzhemechny, F. Choudhery, S.A. Schwarz, S. Ge, K. Shin, J. Sokolov, M.H. Rafailovich, submitted to *Polymer International.*

10. H. J. White, Y. Pu, M. Rafailovich, J. Sokolov, A. H. King, L. A. Giannuzzi, C. Urbanik, B.W. Kempshall, A. Eisenberg, S. A. Schwarz, and Y. M. Strzhemechny, submitted to *Macromolecules.*

Conclusions

Surface sensitive techniques were utilized in this study to investigate phenomena occurring in polymer thin films confined by an interface.

Secondary Ion Mass Spectrometry has been employed to examine polystyrene chain dynamics near attractive surfaces. Diffusion from a silicon surface and from a sputter-deposited carbon surface were compared side by side in tri-layer sandwiches with a deuterated middle layer.

Strong segregation of the deuterated component was observed at the native silicon oxide surface, but was inhibited at the carbon surface, thereby allowing the diffusion behavior to be studied in the latter case over longer annealing times.

A model incorporating segregation effects, and experimental broadening of the diffusion profiles, allowed the depth and time dependence of PS diffusion to be analyzed. A finite element computer program was developed to fit the observed diffusion profiles.

Despite the radically different segregation behavior of dPS at the C surface, the behavior of the diffusion coefficient D was found to be quite similar to the native Si surface. Strong inhibition of chain diffusion has been observed near both surfaces, and diffusion remains inhibited out to distances of several radii of gyration from the surface. D varies with depth superlinearly, scaling roughly as a 3/2-power, which confirms the earlier findings

Importantly, the diffusion coefficient in the marker layer region shows simultaneously a strong time dependence extending over tens of hours. D is

observed to decrease strongly with time at both the vacuum and solid wall surfaces. The surface-induced modification of the film properties appears to propagate from the attractive surface at a rate comparable to that of the diffusing chains.

A consistent mechanism of the depth and time behavior is yet to be formulated. Chain entanglement propagation and/or T_g suppression may be consistent with these results.

Diffusion or segregation behavior near the silicon surface is influenced by the extent of surface oxidation. There is also the potential for remnant moisture at the polymer/silicon interface to influence the redistribution of blend components. The effect of standard wet chemical wafer cleaning procedures on the polystyrene/silicon interface was investigated here. Deuterated solutions were employed to allow detection of remnant moisture from the cleaning/etching steps, and to indicate the extent of hydrogen termination at the polystyrene/silicon interface. The SIMS data indicated that the surface is effectively terminated by approximately one monolayer of hydrogen after an HF etch step, and by a thin oxide layer after an HCl/peroxide etch, in accord with numerous studies.

The use of implant standards and a calibrated polymer blend permitted a rough calibration of the deuterium and fluorine concentrations at the interface, while the oxygen concentration proved difficult to estimate due to the strong effect of oxide formation on SIMS sensitivity. The deuterium and oxygen interfacial peaks were found to be stable under high temperature anneals, and the lack of a CD interfacial peak also indicated that deuterium is associated with the silicon interface and not with the polymer chains. Oxygen and fluorine contamination peaks were also observed at the interface between a floated PS sacrificial layer and the original

PS film surface; these peaks also were stable during the anneals. The widths of the PS/silicon interfacial peaks are resolution limited and the level of deuterium at the interface following the HF etch step was found to be on the order of one monolayer. The level of fluorine coverage is less than 0.01 monolayers. Following exposure to the peroxide/HCl solution, the deuterium level is shown to be much reduced, and the oxygen level is increased, as expected. Despite the wet processes employed in sample preparation, there is no evidence of remnant moisture in the interfacial region.

Surface sensitive techniques were applied to a number of other polymeric thin-film and surface systems. SIMS was used to observe a 'fast exchange' regime in a bilayer melt of lightly sulfonated ionomers. Also, a depth profile was obtained for an interface of PC and a blend of two distinct SAN components, revealing surface segregation of the copolymer with a lower AN content. Immiscible systems of PS/PBrS blends and PS-PVP block colpolymers were annealed for subsequent SIMS studies. In the first case the evidence of PBrS being encapsulated by PS was discovered. In the latter case, the formation of the micelle pattern allowed estimation of the blend enthalpy. XPS was applied to monitor chemical change occurring on the surface of polyethylene pellets as a result of vapor processing/UV exposure. It was found that polyethylene bromination produces two distinct states of bromine, which correspond to two different mechanisms of its attachment. Also, a substantial difference of the sulfuric states was produced by the types of thiolate group used in surface modification reactions.

There are many challenges on the way to gaining a clear picture of interfacial polymer behavior. Systems probed in this thesis and the techniques

applied are quite appropriate for meeting those challenges. Numerous new experiments may be suggested for further studies. Among others, new SIMS measurements on PS/dPS multilayer geometry with an *in-situ* annealing. Utilization of different molecular weights, temperatures, and configurations is desirable. Lateral diffusion SIMS studies may be of great interest. Usage of substrates with varying chemical and physical properties, as well as different types of polymers and fillers, may possibly allow observation and quantification of new interfacial phenomena. Combining SIMS with other powerful techniques such as XPS, AFM, rheometry, etc. will explicate many static and dynamic properties of polymer surfaces.

Appendix: Program for the depth dependence of *D*

'INCSEG.BAS' : An example of a QuickBasic program used among others in this work. "INCRSEG" stands for "INCRemental fitting with SEGregation". This particular code takes into account the $x^{1.5}$ spatial dependence of the diffusion coefficient, and the segregation at the silicon oxide surface. Starting from the given initial condition it calculates least-square fits with a given single experimental profile. Methods and requirements of this program are described in numerous comment statements below.

```
'Declaring subroutines
DECLARE SUB InitialConditions (t, l, w, tot)
DECLARE SUB DiffCoefficient (t, a, nit)
DECLARE SUB MainProcedure (t, tot, s, lam, diff, lamv, diffv, sigma, k, nit, npr)
DECLARE SUB DataOutput (t, k, j, cycle)
DECLARE SUB BoundaryConditions (t, j, lam, lamv, tot, diff, diffv, xo, xr)
DECLARE SUB Convolution (t, sigma, j)
DECLARE SUB DataInput (t, q, npr)

'Declaring functions
DECLARE FUNCTION diffusion (j, i)
DECLARE FUNCTION FindMinimumRight (t, j)
DECLARE FUNCTION ZStarRight (xr, t, j)
DECLARE FUNCTION ExtraTermRight (j, i, lam, lamv, t, tot, diff, diffv, xr)
```

```
DECLARE FUNCTION SegregationRight (j, i, lam, lamv, t, tot, diff, diffv, xr)
DECLARE FUNCTION ChiSquare (t, z)

'Declaring arrays
DIM SHARED c(102, 102)
DIM SHARED d(102)
DIM SHARED f(-300 TO 700)
DIM SHARED g(-300 TO 700)
DIM SHARED h(102, 102)
DIM SHARED lib(102, 102)
DIM SHARED fit(102)
DIM SHARED x(102)

'Input from screen
INPUT "Enter the total thickness of the sample in Angstroms (< 1001) ", th
t = INT(th / 10)
INPUT "Enter the thickness of the dPS layer in Angstroms ", w
INPUT "Enter the thickness of the top hPS layer in Angstroms ", l
INPUT "Enter the diffusion time in cycles ", s
INPUT "Enter the Si-surface correlation length in Angstroms ", lambv
lamv = lambv / 10
INPUT "Enter the relative 'terminal height' of Si-surface segregation ", diffv
INPUT "Enter the instrumental broadening, in Angstroms ", sigm
sigma = INT(sigm / 10)
```

```
INPUT "Enter the number of SIMS profiles you are fitting: ", npr
INPUT "Enter the number of steps for iteration: ", nit
INPUT "Enter the file name with experimental results: ", a$
INPUT "Enter the file name for the initial conditions: ", f$
INPUT "Enter the output name: ", b$
c$ = b$ + "fit.txt"
d$ = b$ + "dat.txt"
e$ = b$ + "min.txt"
OPEN a$ FOR INPUT AS #1
OPEN f$ FOR INPUT AS #5
CALL DataInput(t, q, npr)
CLOSE #1
CLOSE #5
OPEN c$ FOR OUTPUT AS #2
OPEN d$ FOR OUTPUT AS #3
OPEN e$ FOR OUTPUT AS #4
WRITE #3, th, w, l, s, nit, lamb, lambv, diff, diffv, sigm, nit
CLOSE #3

'Primary calculation block
FOR k = 0 TO nit
    CALL InitialConditions(t, l, w, tot)
    CALL DiffCoefficient(t, k, nit)
    CALL MainProcedure(t, tot, s, lam, diff, lamv, diffv, sigma, k, nit, npr)
```

```
NEXT
CLOSE #2
CLOSE #4

'This subroutine defines boundary conditions
SUB BoundaryConditions (t, j, lam, lamv, tot, diff, diffv, xo, xr)
c(j, 0) = c(j, 1)
c(j, t + 1) = c(j, t) - ExtraTermRight(j - 1, t + 1, lam, lamv, t, tot, diff, diffv, xr)
END SUB

'This function calculates the least-square fit parameter χ²
FUNCTION ChiSquare (t, z)
result = 0
FOR n = 0 TO t + 1
    chi = g(n) - h(z, n)
    result = result + (chi * chi)
NEXT
ChiSquare = result
END FUNCTION

'This subroutine convolves generated solution of the diffusion equation with a
'Gaussian
SUB Convolution (t, sigma, j)
COLOR 11, 1
```

```
FOR n = -100 TO -1
    f(n) = 0
NEXT
FOR n = 0 TO t + 1
    f(n) = c(j, n)
NEXT
FOR n = t + 2 TO t + 100
    f(n) = 0
NEXT
PRINT " CONVOLUTION IN PROGRESS!"
pi = 3.14159
FOR i = -20 TO t + 20
    summa = 0
    FOR k = -100 TO (t + 100)
        summa = summa + f(k) * 1 / (SQR(pi) * sigma * EXP(((i - k) ^ 2) /
sigma ^ 2))
    NEXT
    g(i) = summa
NEXT
END SUB

'This subroutine carries out input of experimental data and the files with initial
'conditions
SUB DataInput (t, q, npr)
```

```
FOR i = 0 TO t + 1
    INPUT #1, h(1, i)
    PRINT "i ="; i; "h ="; h(l, i)
NEXT
FOR i = 0 TO t + 1
    INPUT #5, x(i)
    PRINT "i ="; i; "x ="; x(i)
NEXT
CLOSE
END SUB

'This subroutine exports the results of calculations
SUB DataOutput (t, k, j, cycle)
FOR i = 0 TO t + 1
    lib(k * 30 + (cycle - 1) * 10 + j / 10, i) = g(i)
    PRINT k * 30 + (cycle - 1) * 10 + j / 10
    WRITE #3, k, cycle, j, i, c(j, i), g(i), d(i)
NEXT
END SUB

'This subroutine defines depth dependence of the diffusion coefficient
SUB DiffCoefficient (t, k, nit)
FOR i = 0 TO t + 1
    d(i) = ((k / nit) + (1 - (k / nit)) * (1 - i / (t + 1)) ^ 1.5) * .45
```

```
NEXT
END SUB

'This function is responsible for calculating a gradient diffusion part in the
'finite-element algorithm
FUNCTION diffusion (j, i)
diffusion = c(j - 1, i) + d(i) * c(j - 1, i + 1) - c(j - 1, i) * (d(i) + d(i - 1)) + d(i - 1) *
c(j - 1, i - 1)
END FUNCTION

'This function defines an extra term in the equation responsible for surface
'segregation
FUNCTION ExtraTermRight (j, i, lam, lamv, t, tot, diff, diffv, xr)
ExtraTermRight = -(1 / lamv) * (c(j, t + 1) - (ZStarRight(xr, t, j) / t) * ((((tot / 10) -
lam * diff) / (lamv * diffv)) - 1)) * EXP((i - t - 1) / lamv)
END FUNCTION

'This function looks for a point determining the boundaries of the surface excess
'z*
FUNCTION FindMinimumRight (t, j)
xr = t + 1
i = t + 1
DO UNTIL i < t / 2 OR (c(j, i - 1) < c(j, i - 2) AND c(j, i) > c(j, i - 1))
    i = i - 1
```

```
LOOP
IF i = (t / 2) - 1 THEN
    xr = t + 1
ELSE
    xr = i
END IF
FindMinimumRight = xr
END FUNCTION

'This subroutine defines initial conditions
SUB InitialConditions (t, l, w, tot)
   sum = 0
FOR i = 0 TO t + 1
    c(0, i) = x(i)
    sum = sum + c(0, i)
NEXT
tot = sum * 10
END SUB

'This subroutine performs calculations for the main part of the finite-element
'algorithm
SUB MainProcedure (t, tot, s, lam, diff, lamv, diffv, sigma, k, nit, npr)
CALL Convolution(t, sigma, 0)
COLOR 10, 3
```

```
z = 1
a = ChiSquare(t, z)
WRITE #2, k, 0, t + 1, 0, a
FOR cycle = 1 TO INT(s / 1)
    FOR j = 1 TO 100
        sum = 0
        xr = FindMinimumRight(t, j - 1)
        FOR i = 1 TO t
            c(j, i) = diffusion(j, i) + SegregationRight(j, i, lam, lamv, t, tot, diff,
diffv, xr)
            IF c(j, i) < 0 THEN
                c(j, i) = 0
            END IF
            IF c(j, i) > 1 THEN
                c(j, i) = 1
            END IF
            sum = sum + c(j, i)
        NEXT
        CALL BoundaryConditions(t, j, lam, lamv, tot, diff, diffv, xo, xr)
        test1 = ZStarRight(xr, t, j)
        IF INT(j / 10) - j / 10 = 0 THEN
            PRINT "k="; k; "j="; (cycle - 1) * 100 + j
            CALL Convolution(t, sigma, j)
            z = 1
```

```
            a = ChiSquare(t, z)
            WRITE #2, k, (cycle - 1) * 100 + j, xr, test1, a
        END IF
    NEXT
    FOR m = 0 TO t + 1
        c(0, m) = c(100, m)
    NEXT
NEXT
END SUB

'This function is responsible for calculating a surface-segregation part in the
'finite-element algorithm
FUNCTION SegregationRight (j, i, lam, lamv, t, tot, diff, diffv, xr)
SegregationRight = ExtraTermRight(j - 1, i, lam, lamv, t, tot, diff, diffv, xr) * (((d(i
+ 1) - d(i - 1)) / 2) + (d(i) / lamv))
END FUNCTION

'This function calculates surface excess z*
FUNCTION ZStarRight (xr, t, j)
summa = 0
i = t + 1
DO WHILE i > xr
    summar = summar + (c(j, i) - c(j, xr))
    i = i - 1
```

```
LOOP

ZStarRight = summar

END FUNCTION
```

Bibliography

Chapter 1

1. S. A. Schwarz, B. J. Wilkens, M. A. Pudensi, M. H. Rafailovich, J. Sokolov, X. Zhao, W. Zhao, X. Zheng, T. P. Russell, and R. A. L. Jones, *Mol. Phys.* **76**, p.937 (1992).
2. L. C. Feldman, J. W. Mayer, *Fundamentals of surface and thin film analysis*, Elsevier Science Publishing (1986).

Chapter 2

1. A. Doolittle, *J. Appl. Phys.* **22**, p.1471 (1951).
2. M. J. Williams, R.F. Landel, I.W. Ferry, *Amer. Chem. Soc.* 77, p.4701 (1955).
3. P. E. Rouse, *J. Chem. Phys.* **21**, p.1272 (1953).
4. F. Bueche, *J. Chem. Phys.* **22**, p.603 (1954).
5. M. Doi and S. F. Edwards, *The Theory of Polymer Dynamics* (Clarendon Press, Oxford,1986).
6. P. G. de Gennes, *Scaling Concepts in Polymer Physics* (Cornell University Press, Ithaca, 1979).
7. J. M. Deutsch, *Phys. Rev. Lett.* **54**, p.56 (1985).
8. A. N. Semenov, *Physisa A.* **166**, p.263 (1990).
9. M. Rubinstein and S. P. Obukhov, *Phys. Rev. Lett.* **71**, p.1856 (1993).
10. P. Flory, *Principles of Polymer Chemistry* (Cornell University Press, Ithaca, 1971).
11. R. Bruinsma, *Macromolecules* **23**, p.276 (1990).

12. P. A. Thompson, G. S. Grest, and M. O. Robbins, *Phys. Rev. Lett.* **68**, p.3448 (1992).

13. H.-W. Hu and S. Granick, *Science* **258**, p.1339 (1992).

14. J. L. Keddie, R. A. L. Jones, and R. A. Cory, *Europhys. Lett.* **27**, p.59 (1994).

15. W. E. Wallace, J. H. van Zanten, and W. L. Wu, *Phys. Rev. E* **52**, p.R3329 (1995).

16. J. A. Forrest, K. Dalnoki-Veres, J. R. Stevens, and J. R. Dutcher, *Phys. Rev. Lett.* **77**, p.2002 (1996).

17. J. H. van Zanten, W. E. Wallace, and W. L. Wu, *Phys. Rev. E* **53**, p.R2053 (1996).

18. W. Zhao, M. H. Rafailovich, J. Sokolov, L. J. Fetters, R. Plano, M. K. Sanyal, S. K. Sinha, and B. B. Sauer, *Phys. Rev. Lett.* **70**, p.1453 (1993).

19. X. Zheng, B. B Sauer, J. G. Van Alsten, S. A. Schwarz, M. H. Rafailovich, J. Sokolov, and M. Rubinstein, *Phys. Rev. Lett.* **74**, p.407 (1995).

20. O. V. Bychuk and B. O'Shaughnessy, *Phys. Rev. Lett.* **74**, p.1795 (1995).

21. R. Khare, J. J. De Pablo, and A. Yethiraj, *Macromolecules* **29**, p.7910 (1996).

22. A. N. Semenov, *Phys. Rev. Lett.* **80**, p.1908 (1998).

23. B. Frank, A. P. Gast, T. P. Russell, H. R. Brown, and C. Hawker, *Macromolecules* **29**, p.6531 (1996).

24. Y. Liu, T. P. Russell, M. G. Samant, J. Strohr, H. R. Brown, A. Cossy-Favre, and J. Diaz, *Macromolecules* **30**, p.7768 (1997).

25. E. K. Lin, W.-l Wu, and S. K. Satija, *Macromolecules* **30**, p.7224 (1997).

26. X. Zheng, M. H. Rafailovich, J. Sokolov, Y. Strzhemechny, S. A. Schwarz, B. B. Sauer, and M. Rubinstein, *Phys. Rev. Lett.* **79**, p.241 (1997).

27. R. L. Jones, S. K. Kumar, D. L. Ho, R. M. Briber, and T. P. Russell, *Nature* **400**, p.146 (1999).

Chapter 3

1. Y. Strzhemechny, V. Shapovalov, K. G. Zhou, S. A. Schwarz, J. Sokolov, and M. H. Rafailovich, in *Proceedings of MRS 98 Fall Meeting*, (Boston, 1999).
2. Y. Strzhemechny, V. Zaitsev, K. Zhou, S. A. Schwarz, J. Sokolov, and M. H. Rafailovich, submitted to *High Performance Polymers.*
3. G. Coulon, T. P. Russell, V. R. Deline, and P. F. Green, *Macromolecules* **22**, p.2581 (1989).
4. S. J. Whitlow and R.P. Wool, *Macromolecules* **22**, p.2648 (1989).
5. X. Zhao, W. Zhao, J. Sokolov, M. H. Rafailovich, S. A. Schwarz, B. J. Wilkens, R. A. L. Jones, and E. J. Kramer, *Macromolecules* **24**, p.5991 (1991).
6. X. Zheng, B.B. Sauer, J.G. Van Alsten, S.A. Schwarz, M.H. Rafailovich, J. Sokolov, and M. Rubinstein, *Phys. Rev. Lett.* **74**, p.407 (1995).
7. X. Zheng, M. H. Rafailovich, J. Sokolov, Y. Strzhemechny, S. A. Schwarz, B. B. Sauer, and M. Rubinstein, *Phys. Rev. Lett.* **79**, p.241 (1997).
8. X. Zhao, Ph.D. thesis, CUNY (1993).
9. H. Nakanishi and P. Pincus, *J. Chem. Phys.* **79**, p.997 (1983).
10. I. Schmidt and K. Binder, *J. Phys. (Paris)* **46**, p.1631 (1985).
11. R. A. L. Jones, E. J. Kramer, M. H. Rafailovich, J. Sokolov, and S. A. Schwarz, *Phys. Rev. Lett.* **62**, p.280 (1989).
12. P. F. Green and E. J. Kramer, *Macromolecules* **19**, p.1108 (1986).
13. R. J. Composto, J. W. Mayer, E. J. Kramer, and D. M. White, *Phys. Rev. Lett.*

57, p.1312 (1986).

14. Y. Zhang, S. Ge, B. Tang, M. Rafailovich, J. Sokolov, D. G. Peiffer, J. A. Dias, K. O. McElrath, S. Schwarz, and S. Satija, BAPS **44**, No.1, Pt I, p.613, paper KP01 170 (1999).

Chapter 4

1. G. W. Trucks, K. Raghavachari, G. S. Higashi, and Y. J. Chabal, *Phys. Rev. Lett.* **65**, p.504 (1990).
2. X. Zheng, B.B. Sauer, J.G. Van Alsten, S.A. Schwarz, M.H. Rafailovich, J. Sokolov, and M. Rubinstein, *Phys. Rev. Lett.* **74**, p.407 (1995).
3. S. A. Schwarz, B. J. Wilkens, M. A. A. Pudensi, M. H. Rafailovich, J. Sokolov, X. Zhao, W. Zhao, X. Zheng, T. P. Russell, and R. A. J. Jones, *Mol. Phys.* **76,** p.937 (1992).
4. Y. Liu, S. A. Schwarz, W. Zhao, J. Quinn, J. Sokolov, M. Rafailovich, D. Iyengar, E. J. Kramer, W. Dozier, L. J. Fetters, and R. Dickman, *Europhys. Lett.* **32**, p.211 (1995).
5. Y. M. Strzhemechny, S. A. Schwarz, J. Schachter, M. H. Rafailovich, and J. Sokolov, *J. Vac. Sci. Technol. A* **15**, p.894 (1997).
6. J. Phillips, L. Pfeiffer, D. C. Joy, P. P. Smith III, J. M. Gibson, W. M. Augustyniak, and K. W. West, *J. Electrochem. Soc.* **133**, p.224 (1986).
7. D. Graf, M. Grundner, and R. Schulz, *J. Vac. Sci. Technol. A* 7, p.808 (1989).
8. U. Neuwald, *J. Appl. Phys.* **78**, p.4131 (1995).
9. K. Kinoshita and I. Nishiyama, *J. Vac. Sci. Technol.* A **13**, p.2709 (1995).
10. R. A. L. Jones, E. J. Kramer, M. H. Rafailovich, J. Sokolov, and S. A. Schwarz,

Phys. Rev. Lett. **62,** p.280 (1989).

11. Y. Morikawa, K.Kubota, H. Ogawa, T. Ichiki, A. Tachibana, S. Fujimura, and Y. Horiike, *J. Vac. Sci. Technol. A* **16**, p.345 (1998).

Chapter 5

1. C. J. Clarke, A. Eisenberg, J. La Scala, M. H. Rafailovich, J. Sokolov, Z. Li, S. Qu, D. Nguyen, S. A. Schwarz, Y. Strzhemechny, and B. B. Sauer, *Macromolecules*, **30**, 4184 (1997).
2. M. Schaffer, V. Janarthanan, Y. Deng, J. La Scala, L. Guo, M. Rafailovich, J. Sokolov, R. S. Stein, Y. Strzhemechny, and S. A. Schwarz, *Macromolecules* **30**, 1225 (1997).
3. R. H. Colby, X. Zheng, M. Rafailovich, J. Sokolov, S. A. Schwarz, Y. Strzhemechny, and D. Nguyen, *Phys. Rev. Letters* **81**, 3876, (1998).
4. D. Slep, J. Asselta, M. H. Rafailovich, J. Sokolov, D. A. Winesett, A. P. Smith, H. Ade, Y. Strzhemechny, S. A. Schwarz, and B. B. Sauer, *Langmuir*, **14**, 4860, (1998).
5. Y. Strzhemechny, S. A. Schwarz, L. T. Guo, X. Zheng, Y. Liu, J. Sokolov, and M. H. Rafailovich, and D. G. Peiffer in *Secondary Ion Mass Spectrometry. SIMS XI.* ed. G. Gillen, R. Lareau, J. Bennett, and F. Stevie (John Wiley & Sons, New York, 1998), p. 481.
6. N. Chanunpanich, A. Ulman, Y. M. Strzhemechny, S. A. Schwarz, A. Janke, H. G. Braun, and T. Kratzmuller, *Langmiur* **15**, 2089, (1999).
7. N. Chanunpanich, A. Ulman, A. Malagon, Y. M. Strzhemechny, S. A. Schwarz, A. Janke, T. Kratzmueller, and H. G. Braun, *Langmuir* **16**, 3557, (2000).

8. Y. Luo, L. Zeng, W. Lin, B. Yang, M.C. Tamargo, Y.M. Strzhemechny, and S. A. Schwarz, submitted to *Semicond. Sci. Technol.*

9. V. Shapovalov, V. Zaitsev, Y. Strzhemechny, F. Choudhery, S.A. Schwarz, S. Ge, K. Shin, J. Sokolov, M.H. Rafailovich, submitted to *Polymer International.*

10. H. J. White, Y. Pu, M. Rafailovich, J. Sokolov, A. H. King, L. A. Giannuzzi, C. Urbanik, B.W. Kempshall, A. Eisenberg, S. A. Schwarz, and Y. M. Strzhemechny, submitted to *Macromolecules.*